Important Notice

UNIVERSITY OF CALGARY

Estimation of Thomsen's anisotropic parameters from geophysical measurements using equivalent offset gathers and the shifted-hyperbola NMO equation

by

Pavan Kumar Elapavuluri

A THESIS

SUBMITTED TO THE FACULTY OF GRADUATE STUDIES

IN PARTIAL FULFILMENT OF THE REQUIREMENTS FOR THE

DEGREE OF MASTER OF SCIENCE

DEPARTMENT OF GEOLOGY AND GEOPHYSICS

CALGARY, ALBERTA

April, 2003

The undersigned certify that they have read, and recommend to the Faculty of Graduate Studies for acceptance, a thesis entitled "Estimation of Thomsen's anisotropic parameters from geophysical measurements using equivalent offset gathers and the shifted-hyperbola NMO equation" submitted by Pavan Kumar Elapavuluri in partial fulfillment of the requirements for the degree of Master of Science.

Dr. John Bancroft
Geology and Geophysics

Dr. Robert James Brown
Geology and Geophysics

Dr. Richard Klukas
External Examiner
Geomatics Engineering

ABSTRACT

In order to study and understand the complex Earth, exploration geophysicists make many assumptions. One of them is that the Earth is perfectly isotropic while in fact it is fundamentally anisotropic. This faulty assumption results in erroneous imaging of subsurface strata and thus faulty interpretations. To extend the seismic processing techniques to anisotropic media, it is required that we have a measure of the different anisotropy parameters.

In this thesis I propose a method for estimation of Thomsen's P-wave anisotropy parameters (ε and δ) for Vertical Transverse Isotropic (VTI) media using Castle's shifted-hyperbola Normal Moveout (NMO) equation. The method was first tested on a synthetic data and then applied to the field data.

I have shown in this thesis that the shifted hyperbola NMO equation (SNMO) gives better estimate of NMO velocities than Dix's NMO equation, as it is a fourth-order Taylor series approximation while Dix NMO equation is a second-order approximation. A Monte-Carlo Inversion technique was used for the inversion of traveltime data for both NMO velocity and the shift parameter *S*. I have applied this SNMO inversion technique to both Equivalent Offset (EO) and CMP (Common Midpoint) gathers. It was found that the velocity analysis on EO gathers gives comparatively more accurate velocity estimates due to their better signal- to- noise ratio.

After the velocity analysis the NMO velocity and the shift parameter can be used to estimate the anisotropy parameters. I estimated the values of ε and δ on synthetic seismic data. The values of δ were estimated quite accurately while the estimation of the

parameter ε was less accurate. The errors in the estimation of δ varied from 5-10% while the error in estimation of ε varied from 20-30%. I then applied this technique to the field dataset acquired over the Blackfoot Field in Alberta and the anisotropic parameters of formations of interest were estimated and were found compare reasonably with expectations based on known lithology.

Acknowledgements

Completion of this thesis wouldn't have been possible without various contributions of many people. First I would like to express my gratitude to Dr. John Bancroft, who provided a motivating, enthusiastic, and critical atmosphere during the many discussions we had. It was a great pleasure to me to conduct this research under his supervision.

I am highly indebted to many people in CREWES who helped all along the way. Kevin Hall helped in all possible ways. Han-Xing Lu helped me with the ProMAX processing system. Ian Watson was a lot of help while I was interpreting the Blackfoot Field data. I am grateful to Joanne Embelton for proofreading my thesis.

I am thankful to the CREWES consortium for providing me with vital financial support.

I would like to thank my parents for the emotional support they gave me. Last but not the least I would like to acknowledge the support I received from all of my friends, especially Tarun, Sushma, Nilanjan, Anushuya and Harpreet.

TABLE OF CONTENTS

LIST OF FIGURES

LIST OF TABLES

LIST OF SYMBOLS

P	P-mode wave
S	S-mode wave
V_P	P-wave velocity
V_S	S-wave velocity
NMO	normal moveout
SNMO	shifted-hyperbola normal moveout
CMP	common-midpoint
V_{nmo}	normal moveout velocity
V_{int}	interval velocity
V_0	vertical velocity
ε	one of Thomsen's anisotropy parameters
δ	one of Thomsen's anisotropy parameters
τ	two-way zero-offset time
t_0	two-way zero-offset time focusing parameter
2-D	two-dimensional
EO	equivalent-offset
S	shift parameter
λ	Lame parameter
μ	Lame parameter
K	Bulk Modulous

Chapter 1: Introduction

1.1. Introduction

One of the basic assumptions of reflection seismology is that the Earth is perfectly isotropic while it is fundamentally anisotropic (Thomsen, 1986). Exploration seismologists have realized quite early that the assumption of isotropy is not valid in all the cases. Seismic anisotropy can be defined as the dependence of seismic velocity on the direction of [Wavefield] propagation (Sheriff, 2002).

It was realized in several instances that the velocity of seismic waves in the Earth's upper crust varied with the direction of propagation (McCollum and Snell, 1947). Some of the early and more important contributors in this field are Postma (1955), Backus (1962), Helbig (1964), and Berryman (1979).

In recent decades there has been a renewed interest in this field of anisotropy after Thomsen published his paper "Weak elastic anisotropy" in 1986. Some of the other significant contributors in this fields are Grechka *et al.* (1999, 2000), Alkhalifah (1995) and Tsvankin *et al*. (1994, 1995, 1996, 2001).

In spite of the Earth being fundamentally anisotropic, most of the processing algorithms assume the ideal condition of isotropy (Toldi *et al.*, 1999).This faulty assumption leads to erroneous imaging and thus faulty interpretations (Isaac *et al*., 1999). The following are the most commonly observed effects of P-wave anisotropy (seismic anisotropy encountered in P-waves):

- Non-hyperbolic moveout is evident at moderate to large offset to depth ratios.

- DMO corrections fail to properly allow simultaneous imaging of flat and dipping reflectors.

- Significant misties (10-15%) between seismically derived velocities and well-based checkshot velocities are routinely observed.

- Significant errors in depth imaging are observed.

One of the effects of anisotropy is the lateral and vertical mispositioning of the events on a seismic section. These effects are demonstrated in the following figures. Figure 1.1 shows a seismic section migrated using an isotropic migration algorithm. On the other hand Figure 1.2 was migrated using an anisotropic migration algorithm.

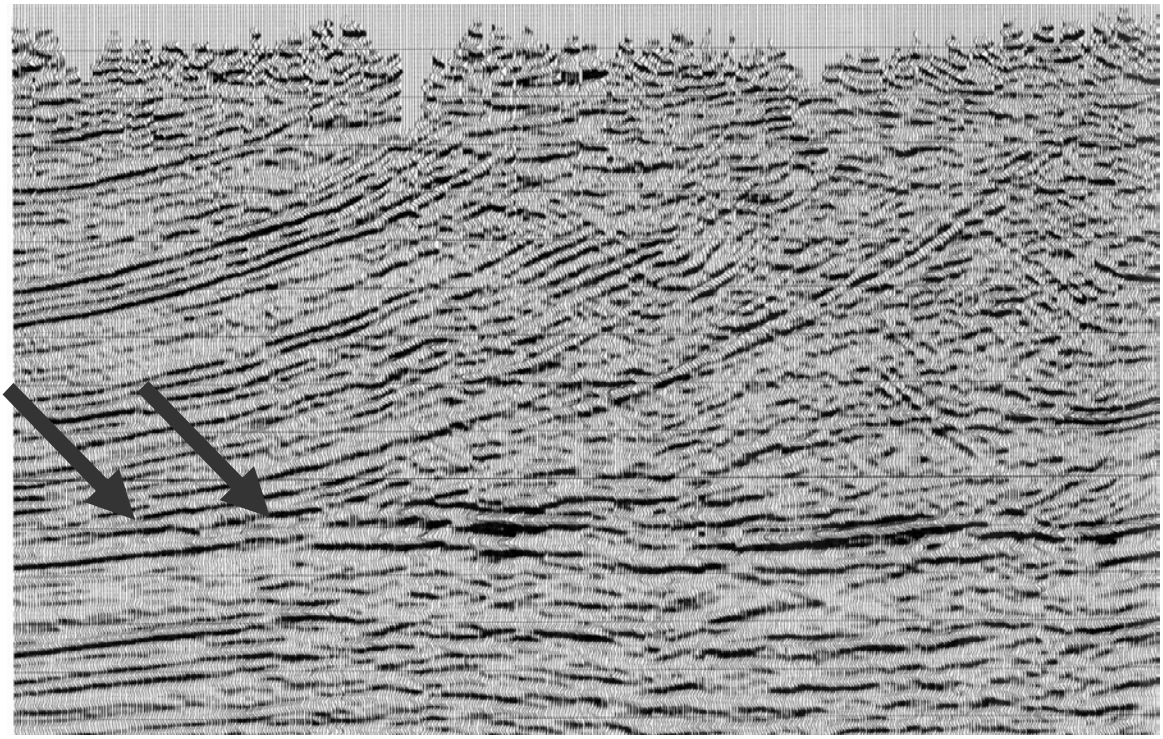

Figure 1.1. Isotropic depth migration (Courtesy Don Lawton).

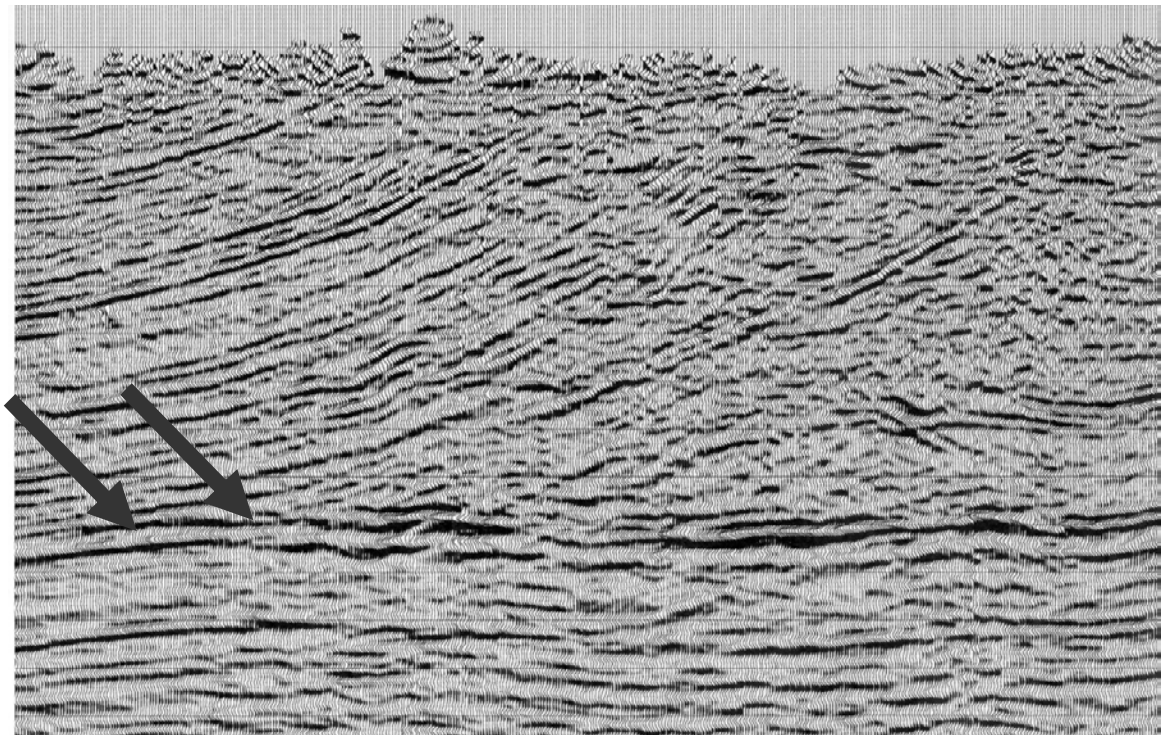

Figure 1.2.Anisotropic depth migration (Courtesy Don Lawton).

It is evident clearly from the Figures 1.1 and 1.2 that the pinchout pointed by two arrows (one arrow showing the position of pinchout before anisotropic migration is applied and the other arrow showing the position after the anisotropic migration was applied) is significantly mispositioned when migrated with an isotropic migration algorithm.

For anisotropy to be taken into account and corrected for, it needs to be quantified and estimated. One of the earliest measures of the P-wave anisotropy is the ratio between the horizontal and vertical P-wave velocities, typically varying from 1.05 to 1.1 and often as large as 1.2 (Sheriff 2002).

Thomsen (1986) introduced a more effective and scientific measure of anisotropy by introducing the constants ε, γ, and δ as effective parameters for the measurement of

anisotropy, where ε and δ determine the P-wave anisotropy and the parameter γ controls the S- wave parameter of anisotropy.

According to Thomsen, δ is the most critical measure of anisotropy in the case of Vertical Transverse Isotropy (VTI) and it doesn't involve the horizontal velocity at all in its definition. Therefore measuring δ is very important for processes like depth imaging. Several authors (Section 1.3) proposed various methods to estimate the parameters of anisotropy.

In this study, the Thomsen parameters ε and δ, are determined from seismic data (both modelled and real) using the shifted-hyperbola NMO equation. The Monte-Carlo inversion technique was used for the inversion of traveltime data for estimating both NMO velocity and the shift parameter. It is also discussed how the parameter estimation on Equivalent Offset (EO) gathers is more accurate than the estimation on CMP gathers.

1.2. Motivation

Determination of δ (the short offset effect) is easy but ε (the long offset effect) is relatively difficult to estimate and requires the knowledge of the horizontal velocity, which is difficult to measure from surface seismic data. In this study, the long offset moveout information is used for ε estimation. Usually Dix-type NMO correction at long offset is not very accurate and causes the hockey stick effect when the effect of anisotropy is strong. The shifted-hyperbola NMO (SNMO) equation is more accurate at longer offsets than the Dix NMO equation (Castle, 1994). Therefore by using the SNMO equation to correct long offset data we get a better estimation of NMO velocity (therefore a better estimate of interval velocity). Due to this accuracy in velocity estimation, we get

a better estimation of ε and δ. It is shown in Chapter 3, that estimation of both the parameters (ε and δ) is heavily dependent on accurate determination of interval velocities.

1.3. Literature review

Theoretical work on seismic anisotropy in exploration seismology dates back to the 1950s. Work done by researchers such as Postma (1955) made the geophysical community take seismic anisotropy seriously. Postma proved that an isotropic-layered Earth behaves as an anisotropic medium if the thickness of the individual layers is finer when compared the wavelength of the seismic waves (long-wave anisotropy). Postma (1955) considered only periodic layering of two types of rocks. Backus (1962) also worked on the same concept of the long wave anisotropy. He extended the work done by Postma (1955**)** to media containing three or more types of rocks. Berryman (1979) also dealt with long-wave anisotropy and concluded that "Anisotropic effects are greatest in areas where layering is quite thin, the wavelengths of seismic signal are greater than the layer thickness and the layers are alternative high and low velocity materials."

Backus (1962) showed that [vertical] transverse isotropy (where one distinct direction often vertical and the other horizontal directions are equal to each other) could be represented by five elastic elements c_{11}, c_{13}, c_{33}, c_{44} and c_{66} of the 6 x 6 stiffness matrix (Nye, 1960). To reduce the number of parameters, Helbig (1981) introduced a normalized, dimensionless set of four parameters, which he called λ, τ, h and k. Hake (1984) calculated these parameters by approximating $t^2 - x^2$ curves over a vertically inhomogeneous TI medium using a three-term Taylor series.

One of the significant papers on anisotropy in exploration seismology is that of Thomsen (1986). In this paper Thomsen shows that the common anisotropy present in nature is transversely isotropic with vertical symmetry axis. He also quantified this anisotropy by defining parameters, namely, ε, δ and γ which are more intuitive, and more easily measurable and implementable than earlier measures of anisotropy.

Knowledge of the anisotropic velocity field is absolutely necessary for the application of processing algorithms that take anisotropy into account. Estimation of Thomsen anisotropic parameters ε, δ and γ, which are necessary for the reconstruction of the anisotropic velocity field have been addressed by various authors.

Byun and Corrigan (1990) used slowness surfaces to calculate the anisotropic parameters over VTI media using VSP data.

Armstrong *et al*. (1995) estimated the anisotropy parameters ε and δ in uniform shale (50 m thick) in the North Sea using walkaway VSP data. They estimated the values of ε and δ as $\varepsilon = 0.17$ and $\delta = -0.03$ over the interval of the VSP. Sena (1991) derived these parameters for azimuthally anisotropic media.

Isaac *et al.* (1998) constructed a scaled physical model to investigate the magnitude of imaging errors incurred by the use of isotropic processing methods. They showed that prestack depth-migration velocity analysis based upon obtaining consistent depth images in the common-offset domain results in the base of the anisotropic section being imaged 50 m (about 3%) too deep.

Grechka *et al.* (2001) discuss the results of the anisotropic parameter estimation on the same physical modelling data. They invert the P-wave NMO velocities and zero offset travel times for vertical velocity V_0 and anisotropic parameters ε and δ. They show that the values of ε and δ match well with the model values

Bozkurt *et al.* (1999) estimated the values of the parameters ε and δ by using vertical velocities from checkshots and horizontal velocities from crosswell tomography along with stacking velocities.

The effect of anisotropy is most prominent on the NMO. As a result numerous authors have analyzed the effect of anisotropy on NMO and devised various techniques to invert the NMO data for estimating anisotropy parameters.

Tsvankin (1995) gave a concise analytic expression for NMO velocities valid for a wide range of anisotropic models including TI media with tilted and in-plane symmetry planes in orthorhombic media. Alkahlifah and Tsvankin (1995) using this NMO expression showed that velocity analysis can be carried out on TI media by inverting the P wave moveout velocities on the ray parameter. They also demonstrate how the influence of stratigraphic anisotropic overburden on the moveout velocity can be stripped through the Dix type differentiation scheme. They study the feasibility of inversion of ε, γ and δ solely from surface seismic data. They came to the conclusion that it would be easier to estimate η (a combination of ε and δ) and $V_{nmo}(0)$, rather than estimating both ε and δ along with vertical velocity $V_p(0)$. Alkahlifah *et al.* (1995) state that η and $V_{nmo}(0)$ are

sufficient for reconstruction of the anisotropic velocity field. The drawback of their method is that it requires a layer with at least two different apparent dips.

The NMO equation used throughout the industry was derived by Dix (1955). This is a short offset (2-term) approximation of the Taylor series expansion of traveltime as the function of offset, given by Taner and Koehler in 1969. Malvicichko (1978) found that Bolshix's (1956) NMO equation constituted the first four terms of Gauss's hypergeometric series, which has an analytic sum and wrote the equation as a compact analytical sum. He rewrote this compact analytical sum in the form of the shifted-hyperbola NMO equation.

Castle (1994) analytically proved that the shifted-hyperbola NMO (SNMO) equation by Malovichko(1978) represents the exact moveout equation as it satisfies the three geophysical requirements of reciprocity, finite slowness and the correspondence with a constant-velocity Earth.

Siliqi *et al.*(2000) used the shifted-hyperbola approach (Castle, 1994) to estimate the anelliptic parameter η (Alkalifah and Tsvankin, 1995).

Velocity analysis is usually performed on CMP gathers (Mayne, 1962). Here the analysis is performed on the EO gathers after Bancroft *et al.* (1998). All the traces in the prestack migration aperture, regardless of the source or receiver position, may be used to form an EO gather. Traces within the EO gather are sorted by equivalent offset. Bancroft *et al. (1998)* also showed that the velocity analysis is more accurate when performed over an EO gather rather than on a CMP gather. The advantages of an EO gather over a CMP gather are discussed in detail in Chapter 3.

This thesis addresses the estimation of Thomsen's anisotropy parameters ε and δ from seismic data. First the method was applied to model data where it is found that estimation of δ was quite accurate whereas estimation of ε was not that accurate. The method is then tested over real data acquired over the Blackfoot field in Alberta.

1.4. Determination of δ

The interval velocities are estimated over the gathers using a highly accurate velocity estimation technique. These are compared with velocities estimated from the sonic log or VSPs to estimate the value of δ. The determination of δ is illustrated in the Figure 1.3.

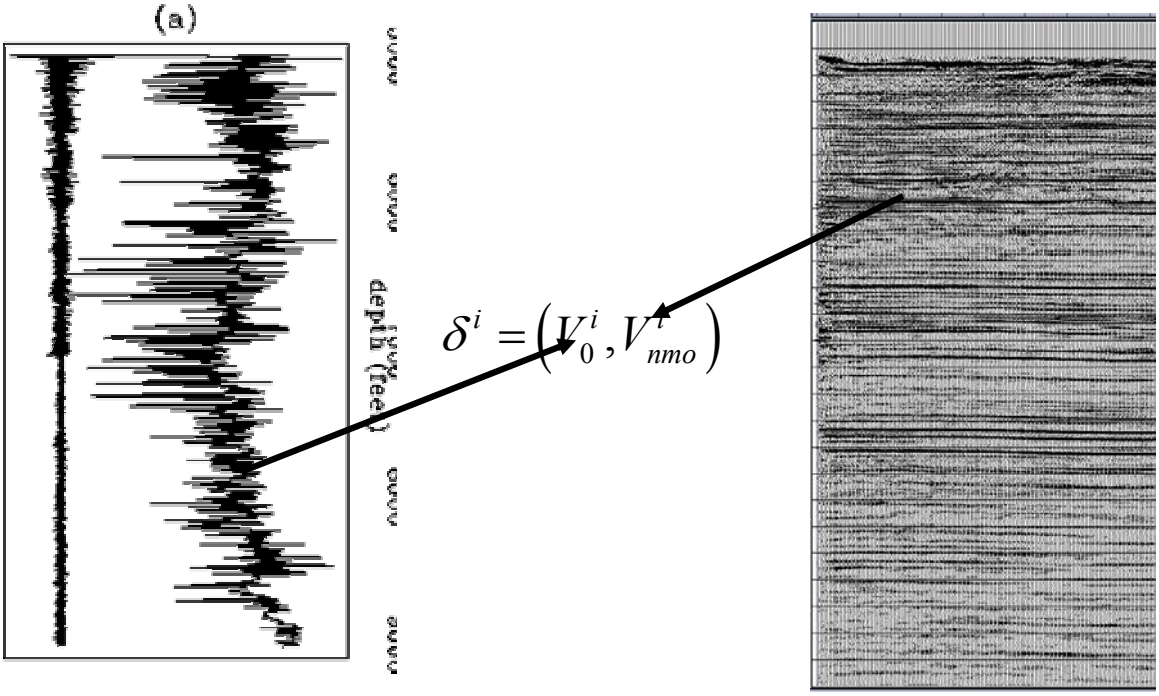

Figure 1.3. The method for estimating δ using wellog/VSP and seismic data

1.5. Determination of ε

The procedure consists of two steps. In the first step, the parameters for normal moveout correction, V_{nmo} and the shift parameter S, are determined using Monte-Carlo inversion over the gathers. In the next step, the anisotropic parameter ε is computed over the data. A relationship that describes the dependency of ε on S, V_{NMO} and V_0 (vertical velocity from well-logs/VSP surveys) is used. This method is illustrated in the Figure 1.4.

The velocities from VSP data are used as the vertical velocities in the case of real data as it is relatively not affected by the effects of velocity dispersion (the dependence of the velocity of the wave on the frequency). On the other hand, well logs that operate at a higher frequency than the surface seismic experiment are affected by this phenomenon.

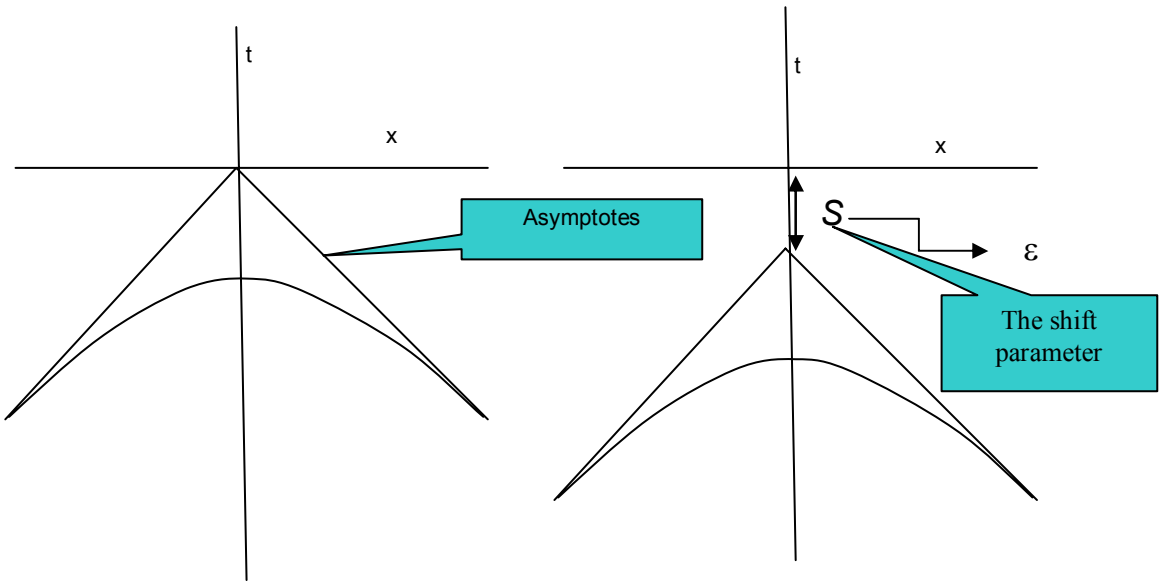

Figure. 1.4. Estimation of ε using the shifted-hyperbola NMO equation.

1.6. Results and conclusions

In this Chapter a method for estimation of Thomsen's P-wave anisotropy parameters (ε and δ) for TI media using Castle's shifted-hyperbola NMO equation has been proposed. The shifted-hyperbola equation gives better estimates of NMO velocities than Dix NMO equation, as it's a fourth-order Taylor series approximation while Dix's NMO equation is a third order approximation.

The Monte-Carlo inversion technique was used for the inversion of traveltime data for the estimation of both NMO velocity and the shift parameter *S*.

This technique was applied on both the equivalent-offset (EO) and CMP gathers. It was found that EO gathers, due to their better signal to noise ratio, gave a better estimation. The values of ε and δ were estimated on synthetic seismic data.

The values of δ were estimated quite accurately while the estimation of ε was less accurate. The errors in the estimation of δ varied from 5-10% while the error in estimation of ε varied from 20-30%.

The technique is then applied to field data acquired over the Blackfoot Field in Alberta and the anisotropic parameters of formations of interest are then estimated.

1.7. Contributions

The contributions of this thesis are as the following:

1. A method for estimation of anisotropy parameters ε and δ is proposed.

2. The difficulty of estimation of ε (which needs a measure of horizontal velocity) is solved by using the extra information (shift parameter *S*) gained by fitting a shifted-hyperbola NMO equation to the large offset traveltime moveouts.

3. The shifted-hyperbola NMO equation is fitted to the traveltime moveouts using the Monte-Carlo inversion and the shift parameter *S* and the V_{nmo} are estimated.

4. The technique is tested on model data and then applied to real data.

Chapter 2: Theory

This Chapter discusses in detail the theoretical background of the concepts used in this study. The concepts discussed in detail are:

1. Elastic anisotropy.
2. Weak anisotropy.
3. Equivalent offset (EO) gather.
4. Dix Normal Moveout (NMO) equation.
5. Shifted hyperbola NMO equation.

2.1 Elastic Anisotropy

Seismic anisotropy can be defined as the dependence of the seismic velocity on the direction or the angle of propagation (Sheriff, 2002). A linearly elastic material is defined as one that obeys Hooke's law. According to this law each component of stress σ_{ij} is linearly dependent upon every component of strain ε_{kl} (Nye, 1957). Since stress and strain components are vectors they can be oriented along any of three axes (*x, y* and *z*) and indices may assume the value of 1, 2 or 3 respectively. Therefore there can be nine such relationships, each involving one component of stress and nine components of strain. These nine equations can be written compactly as

$$\sigma_{ij} = \sum_{k=1}^{3}\sum_{l=1}^{3} C_{ijkl}\varepsilon_{kl}, \quad i,j = 1,2,3 \qquad \text{(Thomsen, 1986).} \qquad (2.1)$$

Newton's second law of motion can be written as :

$$\rho \frac{\partial^2 u_i}{\partial t^2} = \frac{\partial \sigma_{ij}}{dx_j} \ , \tag{2.2}$$

where u_i is the position vector and ρ is the density. Combing Equations (2.2) and (2.1) the wave equation can be written as:

$$\rho \frac{\partial^2 u_i}{\partial t^2} = C_{ijmn} \frac{\partial^2 u_m}{\partial x_n \partial x_j}, \tag{2.3}$$

where the 3×3×3×3 elastic tensor C_{ijkl} characterizes the stiffness of the medium (Nye, 1960) . The inherent symmetry of stress leaves only six independent equations. Giving physical meaning to C_{ijkl}, they can be defined as the requisite stresses to produce the strains ε_{12} and ε_{21}. This can be written as,

$$\sigma_{ij} = C_{ij12}\varepsilon_{12} + C_{ij21}\varepsilon_{21} = \left(C_{ij12} + C_{ij21}\right)\varepsilon_{12} . \tag{2.4}$$

These coefficients in general, always occur together and so are set equal to one another (Nye, 1960). Thus,

$$C_{ijkl} = C_{ijlk} \tag{2.5}$$

and similarly,

$$C_{ijkl} = C_{jikl} . \tag{2.6}$$

This leaves 36 independent coefficients out of the original 81 in the C_{ijkl} stiffness tensor. Similarly, due to the symmetry in strain ε, only six terms are independent. This leads to the introduction of the Voigt recipe, which changes the 3×3×3×3 tensor into a more compact 6×6 matrix. The recipe is as follows:

$11 \rightarrow 1$
$22 \rightarrow 2$
$33 \rightarrow 3$
$32=23 \rightarrow 4$
$31=13 \rightarrow 5$
$12=21 \rightarrow 6$ (2.7)

This 6x6 matrix is symmetric so even in the worst case (triclinic) it has 21 different elements. I will discuss it for couple of symmetries – Isotropy and Vertical Transverse Isotropy (VTI).

Isotropy

Using the above compaction scheme the $C_{\alpha\beta}$ matrix for an isotropic medium can be written as :

$$C_{\alpha\beta} = \begin{bmatrix} C_{11} & (C_{11}-2C_{44}) & (C_{11}-2C_{44}) & & & \\ & C_{11} & (C_{11}-2C_{44}) & & & \\ & & C_{11} & & & \\ & & & C_{44} & & \\ & & & & C_{44} & \\ & & & & & C_{44} \end{bmatrix}. \quad (2.8)$$

Only the non-zero components in the upper triangle are shown for convenience and simplicity, the lower triangle and the upper triangle are identical to each other. The nonzero components are related to the Lamé parameters λ and μ and the bulk modulus, K as given by the equations (2.9) and (2.10).

$$C_{11} = \lambda + 2\mu = K + \frac{4}{3}\mu \text{ and} \quad (2.9)$$

$$C_{44} = \mu . \quad (2.10)$$

It is intuitively obvious at the equation (2.8) that isotropic symmetry is the simplest of all the symmetries. It has only two independent elements. But this symmetry is not usually found in nature.

Vertical Transverse Isotropy

On the other hand a simple, realistic, and frequently encountered case of anisotropy in exploration seismology is transverse isotropy or hexagonal symmetry. It is characterized by one distinct direction, usually vertical and other usually equal horizontal directions. Due to the vertical axis of symmetry, this symmetry is known as vertical transverse isotropy (VTI).

The elastic modulus in the VTI matrix form can be written as (2.11)

$$C_{\alpha\beta} = \begin{bmatrix} C_{11} & (C_{11}-2C_{66}) & C_{13} & & & \\ & C_{11} & C_{13} & & & \\ & & C_{33} & & & \\ & & & C_{44} & & \\ & & & & C_{44} & \\ & & & & & C_{66} \end{bmatrix} \qquad (2.11).$$

It can be noted that the above matrix has five independent elements distributed among twelve nonzero components. In the VTI case the *z*-axis is the unique axis. The differences between the transversely isotropic and the purely isotropic elastic matrices consist of the inclusion of three more elastic parameters, C_{13}, C_{44} and C_{66}. It can be easily proved that isotropy is a special case of VTI when $C11=C_{33}$ etc.

Thomsen anisotropy parameters

The wave equation derived using the equation of motion (Daley and Hron, 1977) can be written as:

$$\frac{\partial^2 u_i}{\partial t^2} = \frac{C_{\alpha\beta}}{\rho}\frac{\partial^2 u_m}{dx_n dx_j}. \qquad (2.12)$$

Daley and Hron (1977) gave the following three independent solutions.

$$\rho V_{\mathrm{P}}^2 = \frac{1}{2}\left[C_{33} + C_{44} + \left(C_{11} - C_{33}\right)\sin^2\theta + D\left(\theta\right)\right], \qquad (2.13)$$

$$\rho V_{\mathrm{SV}}^2 = \left[C_{33} + C_{44} + \left(C_{11} - C_{33}\right)\sin^2\theta - D\left(\theta\right)\right], \text{ and} \qquad (2.14)$$

$$\rho V_{\mathrm{SH}}^2 = \left[C_{44}\cos^2\theta + C_{66}\sin^2\theta\right]. \qquad (2.15)$$

where,

$$D\left(\theta\right) = \left\{\left(C_{33} - C_{44}\right)^2 + 2\left[2\left(C_{13} + C_{44}\right)^2 - \left(C_{33} - C_{44}\right)\left(C_{11} + C_{33} - 2C_{44}\right)\right]\sin^2\theta\right.$$

$$\left. + \left[\left(C_{11} + C_{33} - 2C_{44}\right)^2 - 4\left(C_{13} + C_{44}\right)^2\right]\sin^2\theta\right\}^{1/2}, \qquad (2.16)$$

and θ is the polar angle between the symmetry axis and the direction of propagation.

According to Thomsen not all these elastic moduli need to be determined. Only certain combinations of these affect the data. He defines these combinations as 'anisotropic parameters'. Thomsen parameters are quite suitable in describing the amount of anisotropy present within the TI earth or in a TI model. These parameters are defined as:

$$\varepsilon \equiv \frac{C_{11} - C_{33}}{2C_{33}} \ , \tag{2.17}$$

$$\gamma \equiv \frac{C_{66} - C_{44}}{2C_{44}} \ , \tag{2.18}$$

$$\delta^* \equiv \frac{1}{2C_{33}}\left[2\left(C_{13} + C_{44}\right)^2 - \left(C_{33} - C_{44}\right)\left(C_{11} + C_{33} - 2C_{44}\right)\right], \tag{2.19}$$

and the vertical velocities for the P and S waves defined respectively as

$$\alpha_0 = \sqrt{C_{33}/\rho} \tag{2.20}$$

$$\beta_0 = \sqrt{C_{44}/\rho} \tag{2.21}$$

(Thomsen, 1986). The P wave and S wave (horizontal and vertical polarized) velocities can be written in terms of Thomsen parameters as the following equations:

$$V_{\mathrm{p}}^2\left(\theta\right) = \alpha_0^2\left[1 + \varepsilon \sin^2\theta + D^*\left(\theta\right)\right], \tag{2.22}$$

$$V_{\mathrm{SV}}^2\left(\theta\right) = \beta_0^2\left[1 + \varepsilon\frac{\alpha^2}{\beta^2}\sin^2\theta - \frac{\alpha^2}{\beta^2}D^*\left(\theta\right)\right], \text{ and} \tag{2.23}$$

$$V_{\mathrm{SH}}^2\left(\theta\right) = \alpha_0^2\left[1 + 2\gamma\sin^2\theta\right]. \tag{2.24}$$

where,

$$D^*\left(\theta\right) \equiv \frac{1}{2}\left(1 - \frac{\beta_0^2}{\alpha_0^2}\right)\left\{\left[1 + \frac{4\delta^*}{\left(1 - \beta_0^2/\alpha_0^2\right)}\sin^2\theta\cos^2\theta + \frac{4\left(1 - \beta_0^2/\alpha_0^2 + \varepsilon\right)\varepsilon}{\left(1 - \beta_0^2/\alpha_0^2\right)}\sin^4\theta\right]^{1/2} - 1\right\}. \tag{2.25}$$

(Thomsen, 1986).

2.2 Weak anisotropy

Equations (2.22) - (2.25) are exact but are too complex to be practically useful. Thomsen (1986), states that these equations can be simplified by assuming that most rocks are weakly anisotropic even though the minerals constituting them may be highly anisotropic. This assumption is validated by the data compiled by Thomsen (1986) on anisotropy for a number of sedimentary rocks. The original data consists of both ultrasonic and seismic-band velocity measurements on sedimentary rocks. This data confirms that most rocks are "weak to moderately" anisotropic.

The equations (2.22) - (2.25) can be rewritten for weak anisotropy as the following equations.

$$V_{\mathrm{p}}^2(\theta) = \alpha_0^2\left[1+\delta\sin^2\theta\cos^2\theta+\varepsilon\sin^4\theta\right], \tag{2.26}$$

$$V_{\mathrm{SV}}^2(\theta) = \beta_0^2\left[1+(\varepsilon-\delta)\frac{\alpha^2}{\beta^2}\sin^2\theta\cos^2\theta\right], \tag{2.27}$$

$$V_{\mathrm{SH}}^2(\theta) = \alpha_0^2\left[1+\gamma\sin^2\theta\right], \text{ and} \tag{2.28}$$

$$\delta \equiv \frac{(C_{13}+C_{44})^2-(C_{33}-C_{44})^2}{2C_{33}(C_{33}-C_{44})}. \tag{2.29}$$

The equations (2.26)- (2.29) thus simplified can be easily used to quantify the amount of anisotropy.

2.3 Equivalent Offset (EO) Gather

A scatter point is defined as the point in the subsurface that scatters energy in all directions. The subsurface is approximated by an infinite number of scatter points. The energy from all the sources is assumed to be scattered by the scatterpoint to all the receivers. Each trace contains energy from all the scatterpoints.

According to Bancroft *et al.* (1998), "An EO gather is a collection of energy from all input traces into a 2D space of offset and time where scattered energy is optimally positioned for subsequent focusing operation."

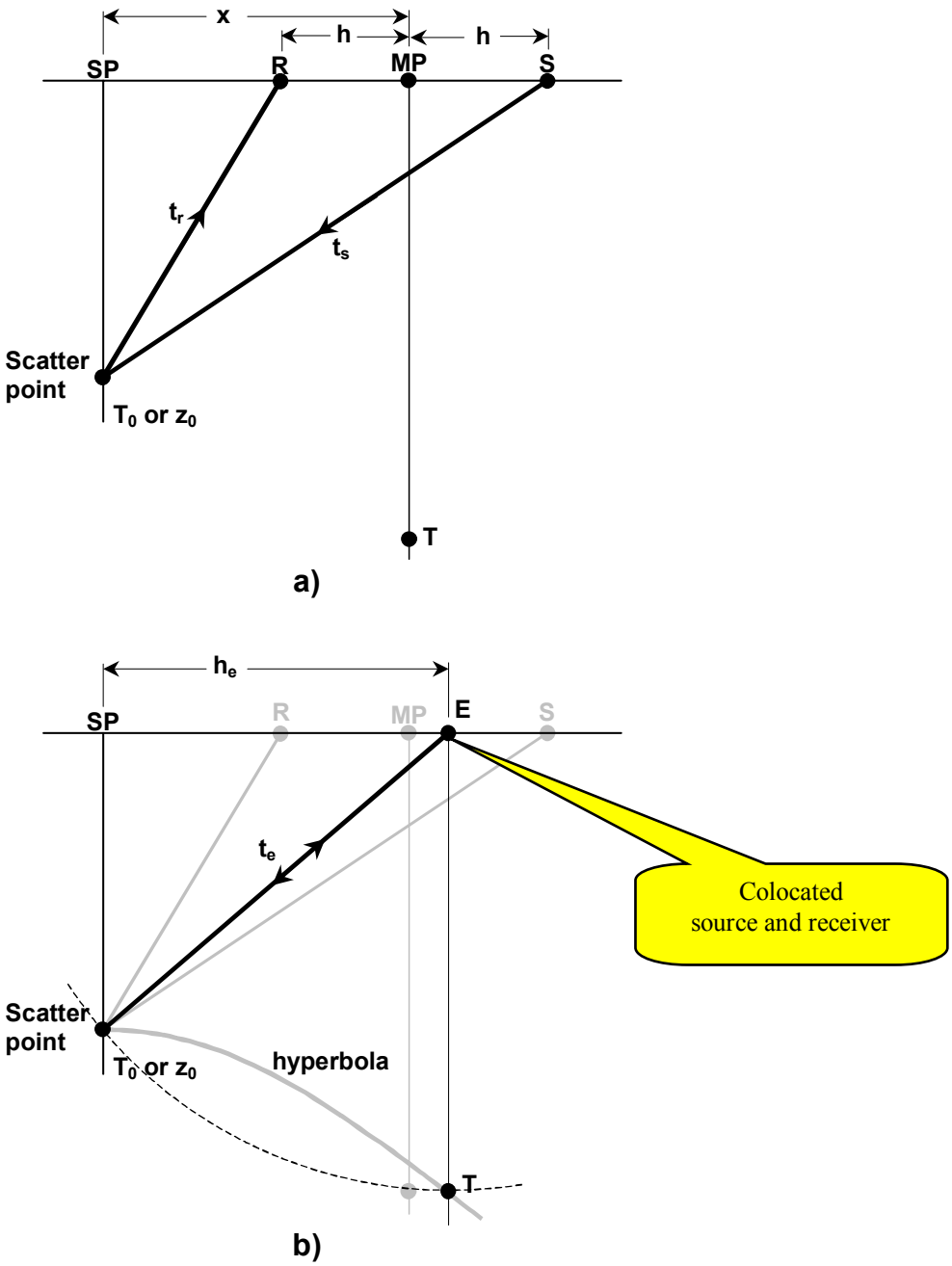

Figure 2.1 Raypaths to scatterpoint a) from a distant CMP, and b) the equivalent offset. (Bancroft, 2002).

In Figure 2.1 the total traveltime from the source to the receiver is given by:

$$t = t_s + t_r . \tag{2.30}$$

From Figure 2.1 assuming a constant velocity medium, Equation (2.30) can be written as

$$t = \left[\left(\frac{t_o}{2} \right)^2 + \frac{(x+h)^2}{V_{rms}^2} \right]^{1/2} + \left[\left(\frac{t_o}{2} \right)^2 + \frac{(x-h)^2}{V_{rms}^2} \right]^{1/2}, \qquad (2.31)$$

(Bancroft *et al.,* 1998).

where t_0 is the two-way traveltime and V_{rms} is the RMS velocity approximation of Taner and Koehler (1969).

Equation (2.29) is known as a double-square-root (DSR) equation and represents the traveltime surface in which the energy from a scatterpoint lies (Bancroft *et al.,* 1998). This surface is known as Cheops Pyramid (Ottaloni *et al*., 1984). The Figure 2.2 shows a Cheops Pyramid for a scatterpoint at ($x = 0$, t_0).

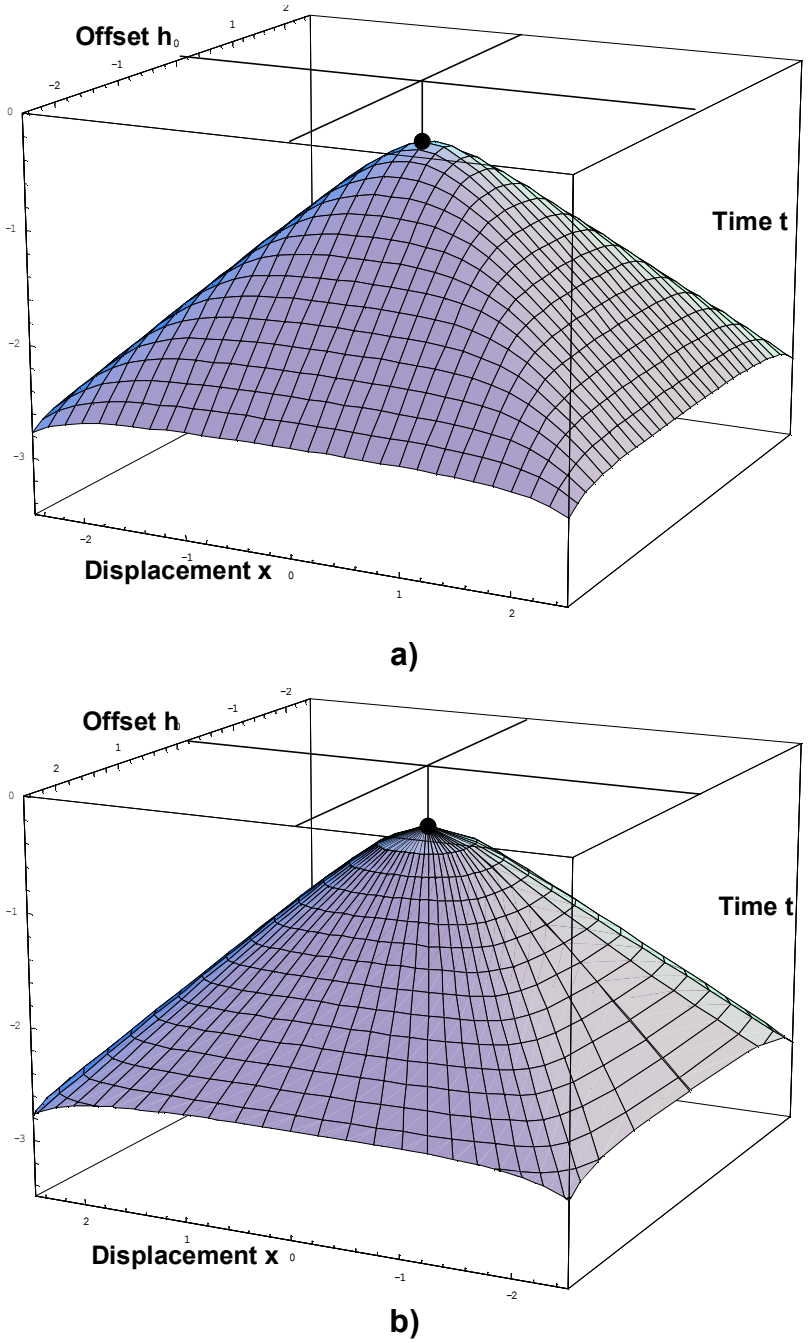

Figure 2.2 Cheops pyramid for continuous range of midpoints and offsets from one scatterpoint is referred to a Cheops pyramid with a) showing a grid in x and h, and b) showing contours at equal times. (Bancroft, 2002)

A CMP gather that is located at the scatterpoint (x=0) intersects Cheops pyramid on a hyperbolic path and allows conventional NMO correction as shown in the Figure 2.2

2.4 The Equivalent Offset

The equivalent offset is defined by converting the DSR equation (2.31) into a single-square- root equation or a hyperbolic form. This is accomplished by defining a new source colocated at the equivalent-offset position E as shown in Figure 2.1. The equivalent offset position, h_e, is chosen to maintain the same traveltime, $2t_e$ as the original path, t as shown in Figure 2.1.

Thus the travel time equation becomes

$$t = 2t_e = t_s + t_r \ . \tag{2.32}$$

Similarly the DSR equation can be written as

$$2\left[\left(\frac{t_0}{2}\right)^2 + \frac{h_e^2}{v_{mig}^2}\right]^{1/2} = \left[\left(\frac{t_0}{2}\right)^2 + \frac{(x+h)^2}{v_{mig}^2}\right]^{1/2} + \left[\left(\frac{t_0}{2}\right)^2 + \frac{(x-h)^2}{v_{mig}^2}\right]^{1/2} \ . \tag{2.33}$$

Equation (2.33) can be simplified into a single square-root-equation by maintaining the same travel time (Bancroft *et al.,* 1998):

$$h_e{}^2 = x^2 + h^2 - \left(\frac{2xh}{tV_{rms}}\right) \ . \tag{2.34}$$

According to Bancroft *et al.* (1998) an input sample can be mapped into an EO gather using the following technique: "When the equivalent offset h_e in the equation (2.32) is considered as a function of x, one input sample at t and h will map to the neighboring EO gathers at constant time and along a hyperbola as shown in the prestack volume of the

Figure 2.2.(as in Bancroft *et al.*, 1998) This equivalent hyperbola represents the path of the input sample as it is mapped to all possible EO gathers".

2.5 Normal Moveout (NMO)

NMO can be defined as: "The additional time required for energy to travel from source to a flat reflecting bed and back to the geophone at some distance from the source point compared with the time it takes to return to the geophone at the source point" (Sheriff, 2002).

The normal moveout equation commonly used to shift events at non-zero offsets to their equivalent zero-offset time is given by

$$t^2 = t_0^2 + \frac{x^2}{V_{NMO}^2} \ , \qquad (2.35)$$

where t is the traveltime at offset x, t_0 is the zero-offset (normal incidence) traveltime, and V_{NMO} is the moveout velocity (Dix, 1955). This is a short offset (2 term) approximation of the Taylor series expansion of traveltime as a function of offset as given by Taner and Koehler (1969) over an isotropic horizontally layered medium. V_{NMO}, which is essentially a parameter that yields the best stack, is commonly used as an approximation for the root mean square (rms) velocity when the media is horizontally layered. For a layered earth model, V_{rms} is given as:

$$V_{rms} = \frac{\sum_{k=1}^{N} \Delta\tau_k V_k^2}{\sum_{k=1}^{N} \Delta\tau_k}, \qquad (2.36)$$

where V_k is the interval velocity and τ_k is the vertical traveltime of the k_{th} layer .

The NMO equation of Dix (1955) is a hyperbola, that is symmetric about the *t*-axis and has asymptotes that intersect at the origin (x =0, t =0). However, for a layered Earth model, Dix's NMO equation is only a small offset approximation.

Castle (1994) proposed the shifted hyperbola NMO (SNMO) equation, which is a better approximation at longer offsets to the moveout than Dix's NMO equation.

2.6 Shifted hyperbola NMO (SNMO) equation

Castle in 1994, published a new approximation to the NMO equation using the three basic principles of geophysics namely reciprocity, finite slowness and exact constant velocity limit. For "reasonable" offsets, his approximation, termed as the shifted hyperbola NMO equation, is given as:

$$t = \tau_s + \sqrt{\tau_x^{\,2} + \frac{x^2}{SV_{NMO}^2}} \quad , \tag{2.37}$$

where $\tau_s = t_0\left(1-\frac{1}{S}\right)$ and $\tau_x = \left(\frac{t_0}{S}\right)$.

In the above equation, the "shift parameter", *S*, is a constant and is described as:

$$S = \frac{\mu_4}{\mu_2^2}, \tag{2.38}$$

where μ_2 and μ_4 are the second and fourth order moments in Taner and Koehler's traveltime expansion. Figure 2.3 shows a comparison between shifted hyperbola and a Dix hyperbola.

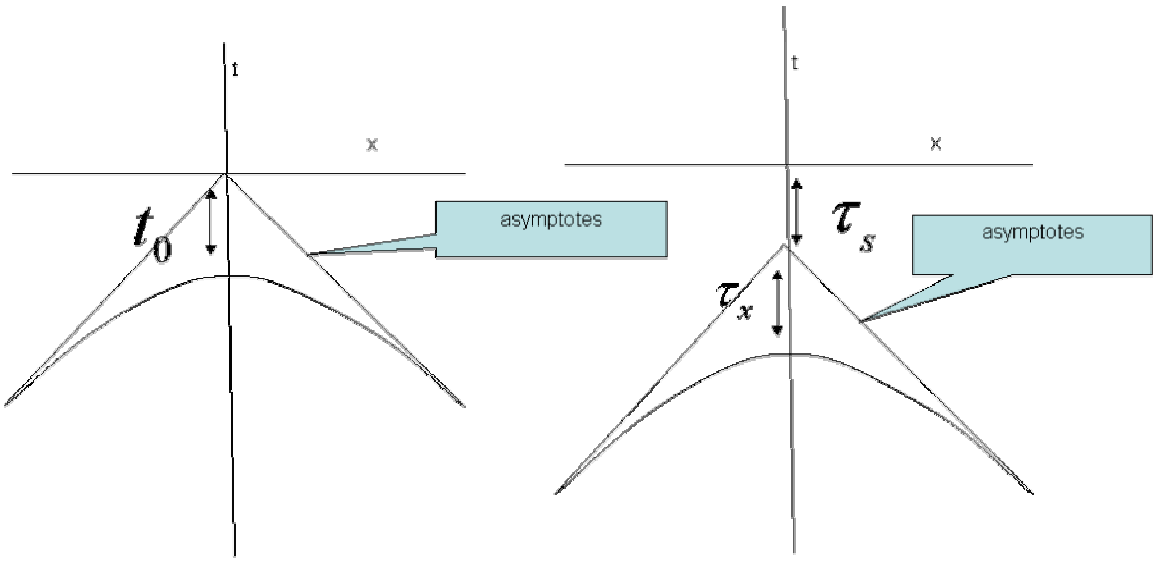

Dix's Hyperbola Shifted Hyperbola

Figure 2.3. Comparison between Dix's hyperbola and a shifted hyperbola.

Although the SNMO with a constant S fits the larger offsets better than Dix NMO formula, Castle (1994) showed that by varying the S with offset, one could obtain a superior fit to the traveltime with a SNMO curve. The most general form of the shifted hyperbola equation is written as:

$$t = \tau_s(h) + \sqrt{\tau_0^2(h) + \frac{x^2}{v^2(h)}} \quad , \tag{2.39}$$

where the parameters τ_S, τ_0 and v are functions of the source-receiver offset (h) as follows:

$$\tau_0(h) = \frac{t_0}{S(h)}, \tag{2.40}$$

$$\tau_S(h) = t_0\left[1 - \frac{1}{S(h)}\right] \text{, and} \tag{2.41}$$

$$v(h) = \sqrt{S(h)}V_{nmo} \quad . \tag{2.42}$$

The offset-dependent shift parameter, *S (h)*, is defined as

$$S(h) = \frac{\frac{h^2}{V_{NMO}^2} - 2t_0(t - t_0)}{(t - t_0)^2}. \qquad (2.43)$$

Castle showed that the general form of an NMO hyperbola is an SNMO through rigourous mathematical proof. SNMO is exact through the fourth order in offset while Dix's NMO equation is only a second order approximation (Castle, 1994). Castle also showed that RMS velocities estimated using the SNMO equation are much more accurate than those estimated using Dix NMO equation.

The earliest formulation of this SNMO is by Bolshix (1956) who derived an NMO equation as a series for the layered earth. Malovichko (1978) unaware of a mistake in Bolshix's equation found out that the first four terms in that equation constituted a hypogeometric series which has an analytic sum. The shifted hyperbola equation as given by Malovichko can be written as:

$$t = t_0\left(1 - \frac{1}{S}\right) + \sqrt{\left(\frac{t_0}{S}\right)^2 + \frac{x^2}{SV_{NMO}^2}} \qquad (2.44)$$

(Castle 1994).

When the Bolsihix traveltime series is compared with the Taner and Koehler's Taylor traveltime series (1969), we see that they differ in their sixth order terms. de Bazelaire (1988) showed that the SNMO is more accurate than Dix's NMO equation by using arguments from geometrical optics. Castle realized that the constants in the equation of de Bazeleaire don't relate to the geology therefore he derived the shifted hyperbola NMO equation in 1994 from 'first principles' and showed that this equation is exact through the

fourth order in offset, while the Dix NMO equation is exact only through second order in offset.

2.7 Comparison of Dix NMO and Shifted-Hyperbola NMO Equations

The first four terms of 'exact' NMO equation for horizontally layered earth as given by Castle (1994) can be written as:

$$t(x) = t_0 + \frac{1}{2t_0\mu_2}x^2 - \frac{1}{8}\frac{\mu_4}{t_0^3\mu_2^4}x^4 + \left[\frac{1}{8}\frac{\mu_4^2}{t_0^5\mu_2^7} - \frac{1}{16}\frac{\mu_6}{t_0^5\mu_2^6}\right]x^6 ..... \tag{2.45}$$

The time series expansion for a shifted hyperbola as given by Castle can be written as

$$t(x) = t_0 + \frac{1}{2t_0\mu_2}x^2 - \frac{1}{8}\frac{\mu_4}{t_0^3\mu_2^4}x^4 + \frac{1}{16}\frac{\mu_4^2}{t_0^5\mu_2^7}x^6 ..... \tag{2.46}$$

Comparing equation (2.44) with the SNMO equation (2.43) shows that the SNMO is exact through the fourth order and the error in the sixth order is given by the following equation:

$$\xi = -\left[\mu_4^2 - \mu_2\mu_6\right]\frac{x^6}{16t_0^5\mu_2^7}. \tag{2.47}$$

According to Castle (1994) the $\left[\mu_4^2 - \mu_2\mu_6\right]$ term in the error expression (2.47) vanishes for a constant-velocity medium and is negligibly small for media with small acceleration, which is true for most geologies; hence the shifted hyperbola gives a very good approximation to sixth order term.

By analyzing the equation, it's trivial to realize that when the shift factor *S* equals 1 the SNMO reduces to Dix's NMO equation. The smaller the shift factor *S* the more deviation there is from Dix's hyperbola.

The Figure 2.4 shows a shifted hyperbola with velocity 3000 m/s and shift parameter *S* varying from 0.1 to 0.9. It is worth noting that when *S* equals to '1', SNMO reduces to a Dix NMO equation.

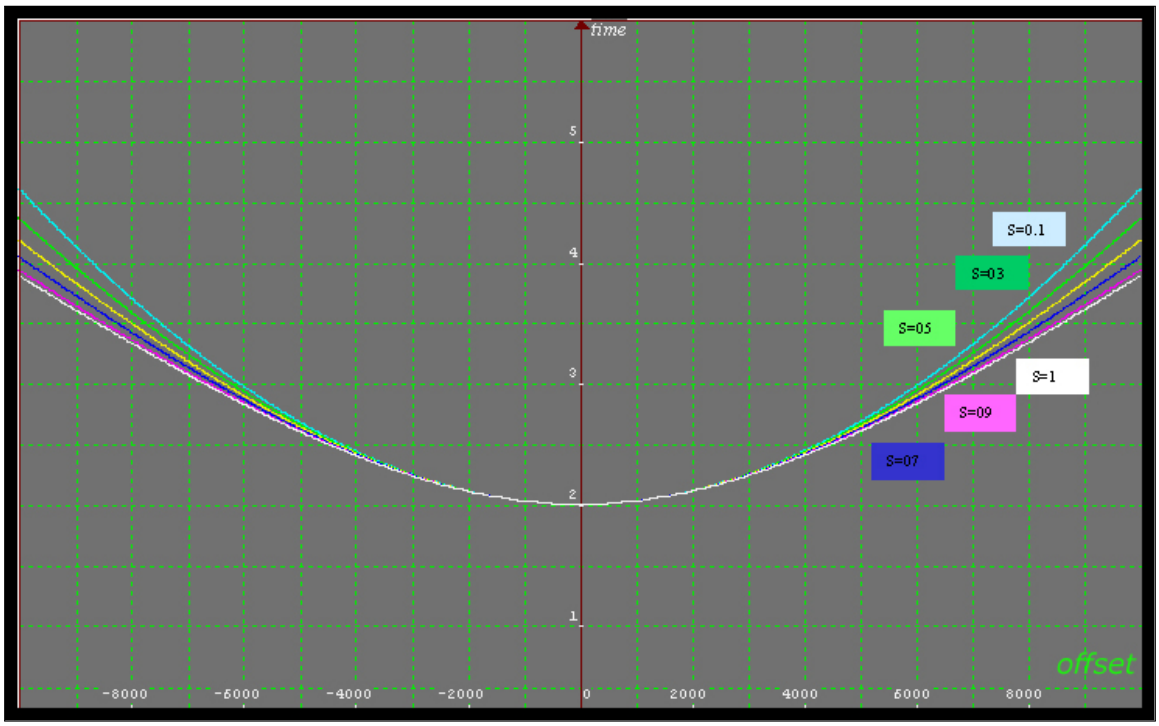

Figure 2.4. The various shifted hyperbolas with varying shift parameter.

The SNMO can be used in exactly the same way as Dix's NMO equation for velocity analysis. Castle (1994) states that the SNMO with a constant shift can be used for the velocity analysis of shorter offset data with a greater accuracy than the Dix NMO equation. In the case of very long offsets, it may be necessary to vary the shift with offset

to obtain a better fit. But the SNMO equation with a constant shift is better than a Dix hyperbola NMO equation.

Castle (1994) applied velocity analysis over a two-layered model using the SNMO with shift varying with offset, the SNMO with constant shift and a Dix NMO equation. He showed that the SNMO with its shift varying with offsets gives the best estimation of RMS velocities followed by constant shifted SNMO and Dix NMO equation.

2.8 Shift parameter *S* and the anisotropy parameters

The shift parameter *S* can be used to estimate the anisotropy parameters as given by:

$$\delta_n = \frac{1}{2}\left(\frac{V_{NMOn}^2}{V_{0n}^2} - 1\right) \tag{2.48}$$

$$\varepsilon_n = \delta_n + \left(\frac{H_N\left(1-k^2\right)}{8V_0^4\left(1-k^2+2\delta_n\right)}\right) \tag{2.49}$$

The derivations of Equations (2.48) and (2.49) and the definitions of the symbols used are discussed in detail in Appendix 1.

In this study, the constant shift parameter, *S*, and V_{NMO} are computed using Monte-Carlo inversion, a non-linear technique. I have derived the relationship between the *S* and Thomsen parameters (ε and δ) and it is then used to determine the anisotropy parameters.

Chapter 3: Synthetic Modelling

In this chapter the method proposed in Chapter 2 will be applied over a synthetic seismic data set. The theory of seismic modelling will be discussed in brief. The methodology adopted for the anisotropic seismic modelling will also be discussed**.**

3.1 Approaches to Seismic Modelling

The generation of synthetic seismograms over a known geological 'mathematical' model is known as mathematical seismic modelling. The data is generated by solving the wave equation in the model. Data thus generated by numerical modelling of wave propagation is very important in exploration seismology. Seismic modelling has many applications; one of them is for the testing and quality control of data processing algorithms. The finite difference and raytracing techniques are the two most frequently used modelling techniques. Raytracing is used in this study to generate anisotropic synthetic seismograms.

3.2 Finite difference Techniques

Finite difference is a numerical technique used to solve the partial differential equations at a point. Starting at the sources energy is propagated on many grid points through the structure to the receivers. Finite-difference techniques can be computationally intensive compared to other techniques such as raytracing.

3.3 Raytracing Techniques

Raytracing techniques are primarily due to the Prague school of Ray Theory (Cerveny, 1985). These techniques trace the path of the seismic rays from the source to an interface

and then on to the receivers. They are used to calculate traveltime and amplitudes tied to the first arrival, the maximum energy arrival or a combination of the seismic wave propagation in the layered medium.

Types of Rays

Raytracing theory uses two families of rays. They are geometrical rays and diffracted rays.

The rays following Snell's law of reflection and transmission at all interfaces are known as geometrical rays, the rays following Keller's law (Norsar 2D Manual) of edge diffraction at a diffraction point are known as diffracted rays. More information on raytracing theory can be found in Cerveny (1985).

Raytracing is a very useful technique for modelling seismograms. It has many advantages such as being easy to implement, it is faster than the finite-difference techniques and can be very accurate. Raytracing theory, however, has some limitations. Care has to be taken before applying this theory so that these pitfalls can be avoided. These limitations will be discussed in detail.

The *Norsar 2D* modelling package was used to model the seismic data. *Norsar 2D* is raytracing program that works on the ray theory proposed by Cerveny (1985).

3.4 Limitations of Raytracing techniques

Two important limitations of ray theory, the assumption of high frequency and smooth interfaces and will now be discussed in more detail.

1. Raytracing is only valid for high frequencies

Raytracing techniques are based on high frequency approximations to the wave theory (Cerveny, 1985). Mathematically this means that this theory is valid only for infinite high frequencies. This means that it assumes that the properties of the medium which is being imaged vary smoothly when compared with the ray for transmission proposes, but except at a reflector interface where we assume a sudden change. This same restriction applies to finite difference methods also, to prevent grid dispersion. In practice, this imposes a restriction on the geological model on which the raytracing should be performed. According to the *Norsar 2D* manual this means that "the seismic wavelength should be shorter than the length of smallest details in the model." In practical terms it must be considerably smaller than quantities such as

- radius of curvature
- the length of the interface
- the layer thickness
- measures of inhomogeneity of material property in the layer.

The values of the quantities depend on the frequency of the probing wavelet (~5—125 KHz) and the velocities of the medium (~500-8000m/s).

2. The Interfaces should be 'smooth'

The interfaces should be smoothed for the ray theory to be valid when the interface which is being imaged is not smooth, or when the interface normal and the interface curvature are fluctuating significantly (within few seismic wavelengths).

3.5 Seismic Modelling Procedure

Synthetic seismograms are generated by the *'Norsar 2D'* software package in the following sequence

1. building up a geologic model
2. specifying the geometry of the survey
3. 'shooting' the seismic rays from the source and generating an event file.
4. generating the synthetic seismogram by filtering this event file with a wavelet.

1 Geologic Model

A layered geological model was built consisting of 9 horizontal interfaces. The model was built in the depth domain and is 6 km deep. The thinnest layer is of thickness 0.5 km with a velocity of 1000 m/s. A 40 Hz zero phase Ricker wavelet was used for the generation of seismograms. The wavelength of the seismic wavelet in this interval is 25m and is much less than the thickness of the particular layer (500 m). It can be therefore be concluded that one of the main conditions of ray theory is valid for this model.

Anisotropy is introduced into the model by assigning Thomsen's anisotropy parameters ε and δ for each layer.

Figure 3.1 shows the layered model with Table 3.1 showing the values of the material properties of this model.

1. P-wave velocity
2. S-wave velocity
3. Density
4. ε and
5. δ

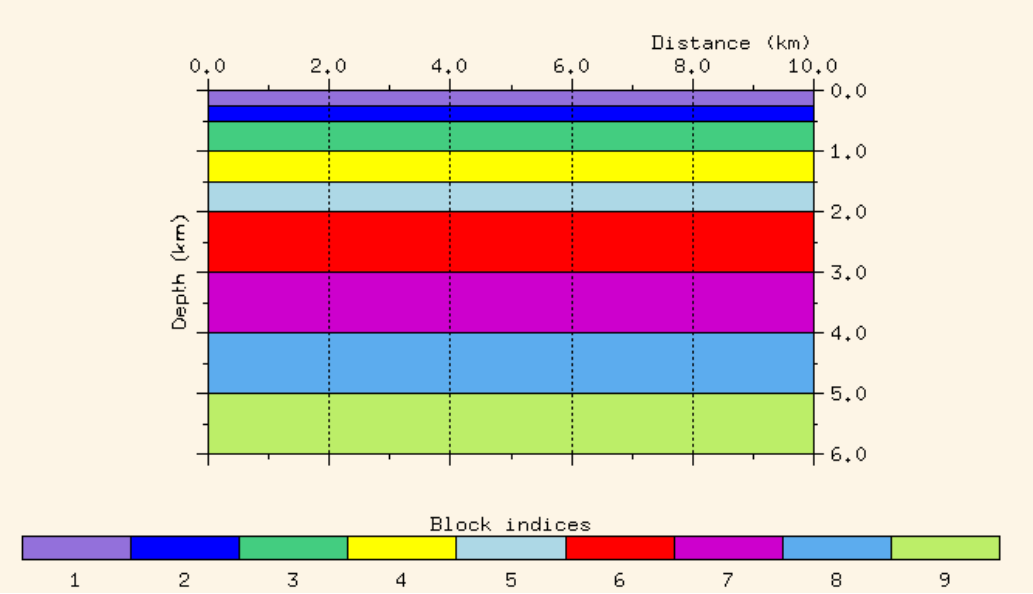

Figure 3.1. The geological model.

Table 3.1. Material properties of the model used.

Interface	P-velocity m/s	S –velocity m/s	Density	ε	δ
1	1000	500	1.1	0	0.2
2	1200	600	1.2	0.05	0.25
3	1500	750	1.3	0.1	0.3
4	2000	1000	1.5	0.15	0.1
5	2500	1250	1.7	0.2	0.15
6	3000	1500	1.9	0.25	0.2
7	4000	2000	2.2	0.3	0.25
8	5000	2500	2.4	0.2	0.3

2 Geometry of the Survey

The geometry of the survey of the seismic modelling experiment is shown in the Figure 3.2. The spread was from -10 km to +10 km. There are 75 shots in total with a shot spacing of 40m. There are 301 receivers for each shot with a receiver spacing of 20m. The circles in Figure 3.2 indicate the position of shots and the triangles indicate the position of the receivers. The type of shooting is with receivers both left and right of the shot.

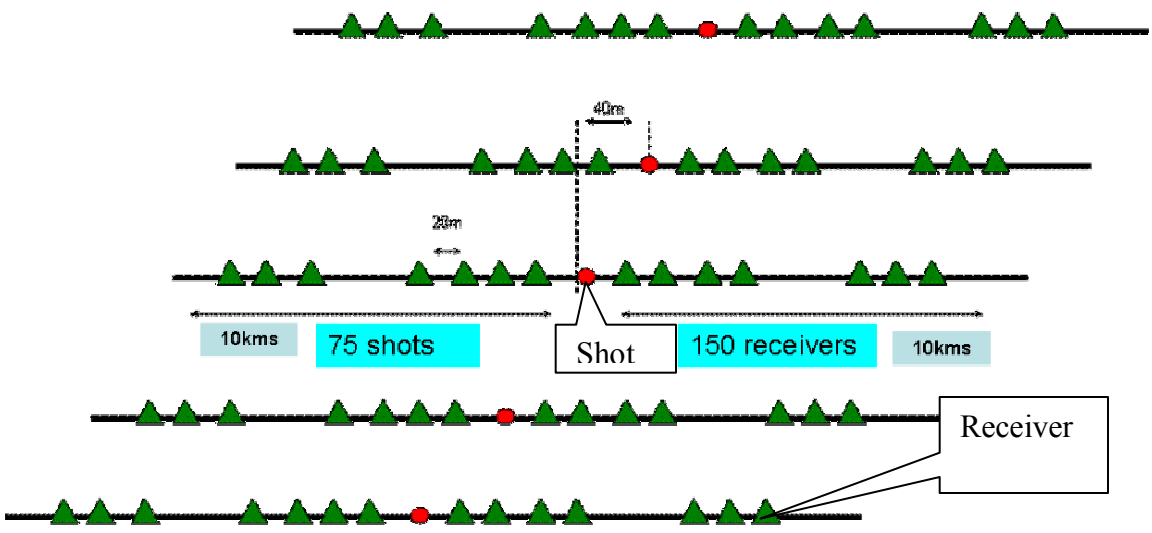

Figure 3.2. The geometry of 2Dthe survey. The different lines indicate the progression of shot and active receivers down a 2D line.

3 Shooting the seismic survey

In practice the rays were traced from the shot to all the receivers. An event file was then generated. This event file has the amplitude and the traveltime information. Figure 3.3 shows the raytracing in progress. The rays are traced from the shot point to all corresponding receivers.

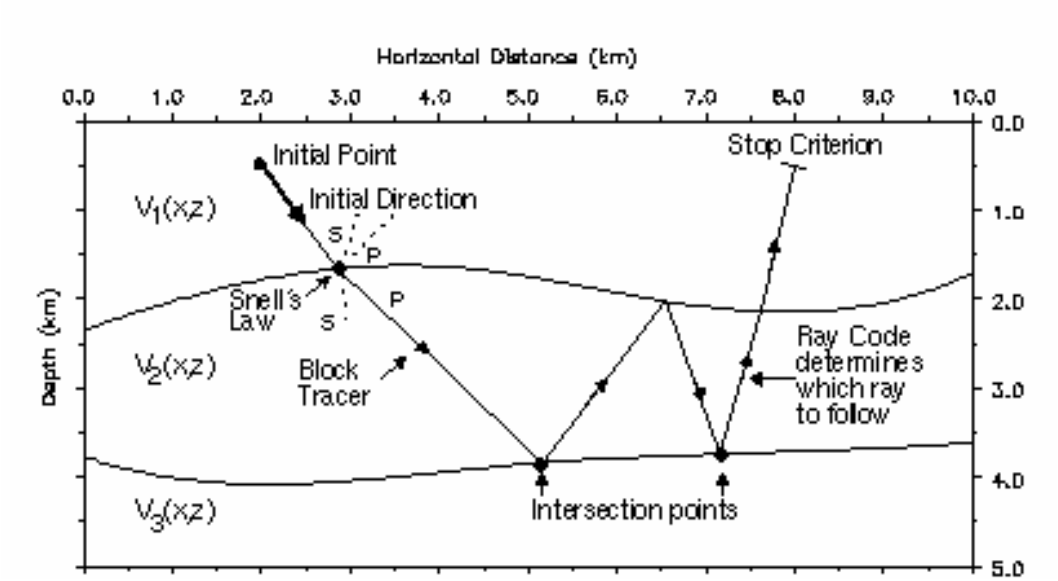

Figure 3.3. Raytracing through the model. (The *Norsar 2D* Manual).

4 Generation of Synthetics

The event file generated by raytracing through the model was convolved with a 40 Hz zero phase 'Ricker' wavelet to generate the synthetic seismogram. Figure 3.4 shows the shot gather from the surface location at -1.0 km.

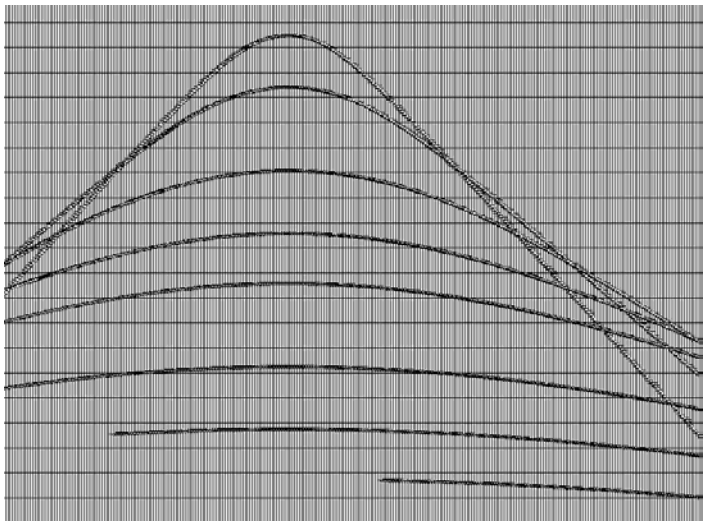

Figure. 3.4. Shot gather at surface location -1.0 km.

The method for anisotropy parameter estimation as discussed in Chapter 2 is then applied to this data. This procedure is discussed in detail below.

3.6 Anisotropy Parameter Estimation

The model data generated above was used to test the estimation method described in Chapter 2. A basic processing flow was applied to the data which is as follows:

1. geometry allocation
2. AGC (Automatic Gain Correction)
3. bandpass filtering
4. sorting into CMP and EO gathers.

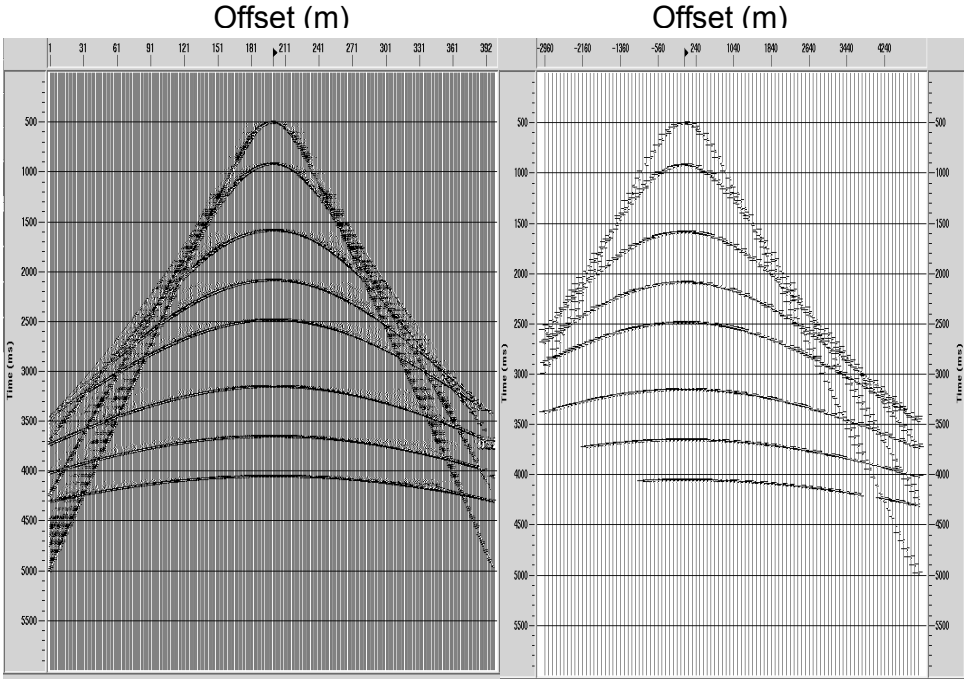

EO gathers CMP Gathers

Figure 3.5. Comparison between CMP and EO gathers.

Using the Monte-Carlo method, the travel time data for each reflectors moveout was inverted for V_{nmo} and S.

3.7 Monte-Carlo Inversion

The shifted-hyperbola equation constitutes a non-linear problem so the linear inversion techniques (e.g. least-square inversion) fail. A random-walk technique like the Monte-Carlo inversion, would serve the purpose of inverting the moveout equation (2.25) for both S and V_{nmo}. The theory of Monte-Carlo inversion is discussed in detail in Appendix 2.

The offset-traveltime moveout information of each significant reflector is used for this inversion.

The model space to be inverted for in this case can be written as $\mathbf{m}(S, V_{nmo})$. One of the advantages of this inversion technique is that it gives good control on both the range of solutions in the model space and the acceptable error range.

Monte-Carlo inversion needs an initial guess for the range of model parameters in which the solution falls. Initially, a very broad range of model values is specified as the search window along with a very large acceptable error. This range is refined at each run and the acceptable error range is also trimmed. This operation is repeated until the error converges at minima acceptable to the user and then the final model is accepted.

- Equation (A1.10) is used to estimate the 'interval velocities'
- The value of V_0, the vertical velocity is determined from the VSP data/sonic logs.

- Equation (2.48) is used to calculate δ_n.

- Equation (2.49) is used to calculate ε_n.

The values of ε and δ were calculated on both CMP and EO gathers .

CMP gathers

Table 3.2 shows the V_{nmo} and S estimated over the CMP gathers. The values of δ and ε were calculated using the NMO velocities. The values are tabulated in Tables 3.3 and Table 3.4 respectively. The estimated values of δ are compared with the model values and the values estimated on the EO gathers are shown in Figure 3.7.

EO gathers

Table 3.2 shows the V_{nmo} and S estimated over the EO gathers. The values of δ and ε were calculated by using the NMO velocities and the shift parameter S estimated on these gathers using the method described above.

The values of ε and δ estimated from both EO and CMP gathers are tabulated in Tables 3.3 and 3.4 respectively.

The significance of these results is that they demonstrate the superiority of the inversion of velocities over EO gathers when compared to the CMP gathers and is essentially the main objective of this thesis.

Table. 3.2. The V_{NMO} and S values estimated from the CMP and EO gathers

layer	V_{nmo} (m/.s) CMP	Shift S CMP	V_{nmo} (m/s) EO	Shift 'S' EO
1	968	0.8134	1237	0.5784
2	1118	0.7999	1336	0.3456
3	1319	0.7868	1828	0.6734
4	1504	0.6942	2290	0.6234
5	1702	0.7198	2908	0.7345
6	1814	0.8517	3655	0.9234
7	2432	0.6863	5059	0.5647
8	2868	0.7107	6259	0.8768

In the EO gather the moveout in each layer is fitted with both the Dix hyperbolic equation and a Castle's shifted- hyperbola equation and corrected for the NMO. The time residual in both the cases is plotted in Figure 3.6. It can be easily verified that the residuals after correction with the shifted-hyperbola NMO equation are much less than those of Dix's equation.

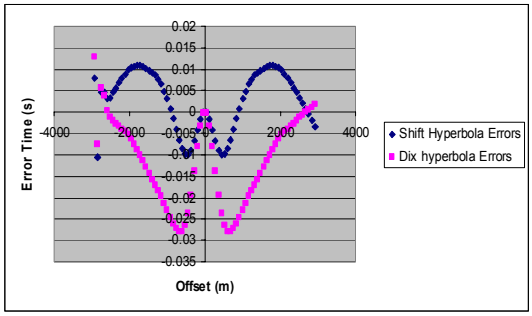

NMO error plot for 2nd interval

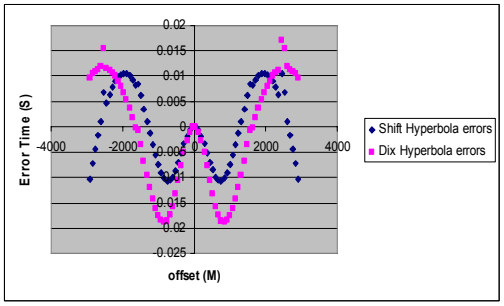

NMO error plot 3rd interval

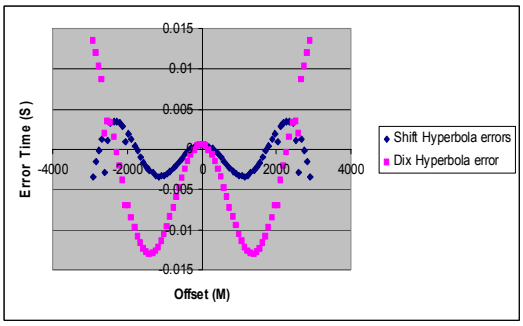

NMO error plot for 4th interval

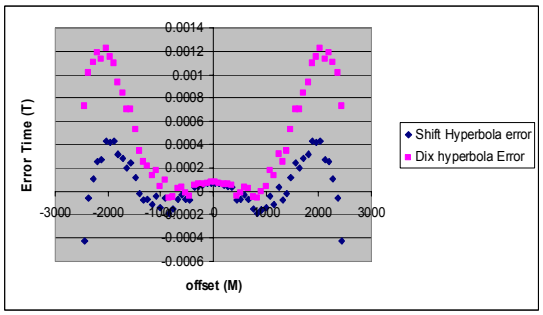

NMO error plot for 5th interval

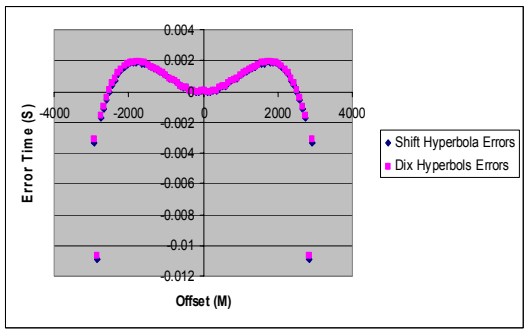

NMO error plot for 6th interval

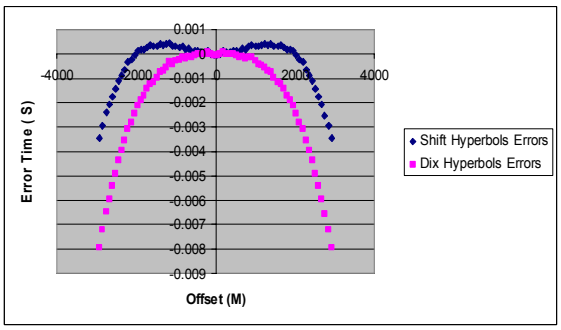

NMO error plot for 7th interval

Figure 3.6. The time residuals in each interface after NMO correction.

The estimated values of δ are compared with the model values and the values estimated on the CMP gathers in Figure 3.7. The estimated values of ε are compared with the model values are shown in Figure 3.8.

3.8 CMP vs. EO Gathers

The values of δ were estimated for this model using both CMP and EO gathers. Figure 3.7 shows a plot of the estimated values of δ. It is evident from the plot that the values estimated from the EO gather match very well with the model values while the CMP values show considerable mismatch. The reason for this mismatch is that the estimation of both δ and ε depend heavily on the accuracy of the RMS velocities. EO gathers give us a better control over velocity estimation than the CMP gathers. The same logic was used for the estimation of ε (Figure 3.8).

The need for the accurate velocities is illustrated with equation (3.1) which shows that the estimation of ε depends on the fourth power of the velocity.

$$\varepsilon_n = \delta_n + \left(\frac{H_N \left(1 - k^2\right)}{8V_0^4 \left(1 - k^2 + 2\delta_n\right)} \right) \tag{3.1}$$

Table 3.3. The values of δ estimated from both CMP and EO gathers are compared with model values.

layer	δ Model	δ CMP	δ EO
1	0.2	0.26	0.19
2	0.25	0.11	0.22
3	0.3	0.24	0.28
4	0.1	0.15	0.09
5	0.15	0.17	0.17
6	0.2	0.24	0.2
7	0.25	0.29	0.24
8	0.3	0.28	0.31

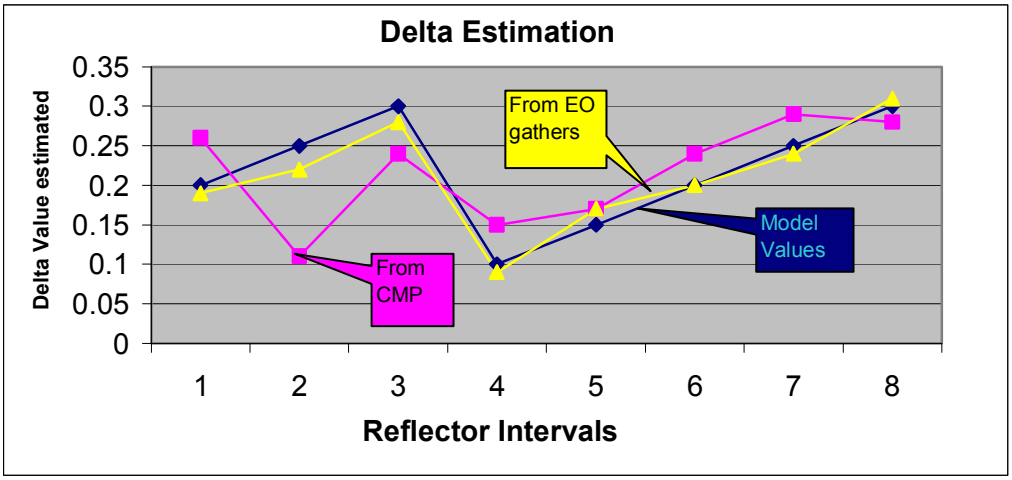

Figure. 3.7. The δ values estimated from CMP and EO gathers compared to model values.

Table 3.4. The values of ε estimated over both CMP and EO gathers are compared with model values.

Layer	ε Model	ε EO	ε CMP
1	0.25	0.18	0.10
2	0.3	0.29	0.22
3	0.15	0.13	0.08
4	0.2	0.20	0.34
5	*0.2*	*0.84*	*0.67*
6	*0.25*	*0.64*	*0.00*
7	*0.3*	*1.34*	*0.48*
8	*0.2*	*1.56*	*0.597*

The values in layers 5-8 (in italics) are non reasonable values as they fall out of the expected range.

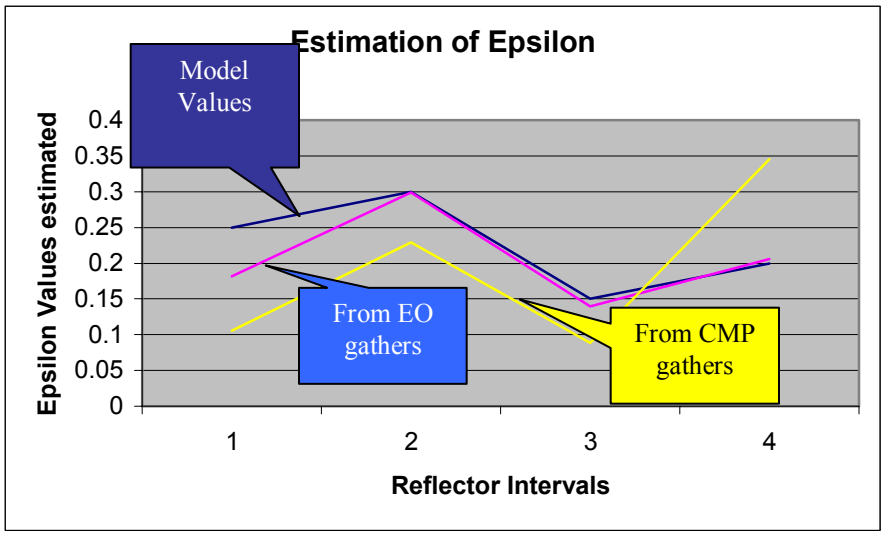

Figure. 3.8. The ε values estimated over CMP and EO gathers are compared to model values.

To evaluate the dependency of accuracy of RMS velocity estimation on the accuracy of the anisotropic parameter estimation, the following error analysis was done.

3.9 Error analysis

The values of the estimated parameters are heavily dependent on the velocities estimated from the Monte-Carlo velocity analysis. A simple error analysis was done by introducing an error into the RMS velocities estimated from the EO gather, and then the values of δ were calculated at each error level using equation (3.2).

$$\delta_n = \frac{1}{2}\left(\frac{V_{NMOn}^2}{V_{0n}^2} - 1\right) \tag{3.2}$$

The results are shown in the Figure 3.9. , where it can be seen in that Figure that for a range of 0-10% error in estimated RMS velocities, a range of 10-120% error was encountered in the values of δ estimated. Bancroft (1998) showed that the velocities

estimated from the CMP gathers may have an error of at least 10%. It is evident from Figure 3.9 that with the 10% error in velocity the anisotropic parameters estimated may have errors which are not acceptable. As the velocities estimated from an EO gather are more accurate, δ and ε values may be estimated with better acuracy using the EO velocities.

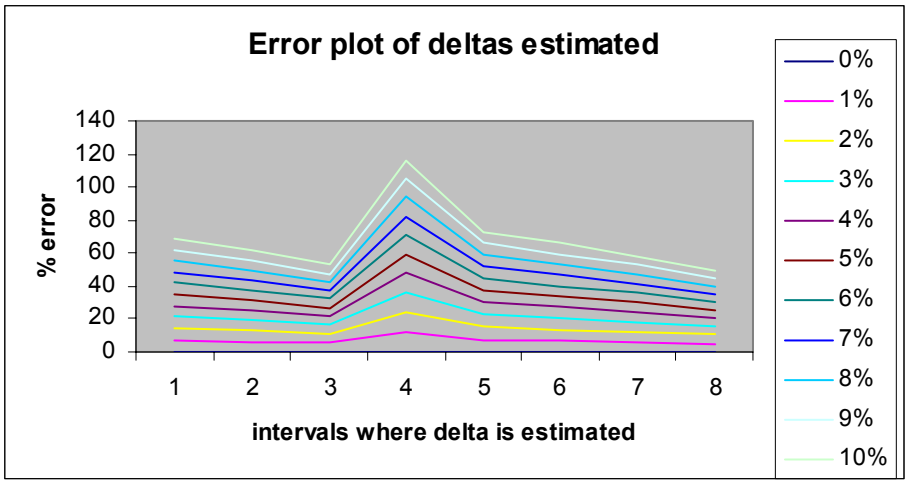

Figure 3.9. Errors in δ encountered due to errors in the estimated velocities.

3.10 Conclusion

The technique for the estimation of anisotropy parameter as discussed in Chapter 2 has been applied to a synthetic seismic dataset generated for an anisotropic model. The anisotropic data has been acquired over a smooth horizontally layered model. Both the CMP and EO gathers were formed at a CMP which has maximum fold coverage. The estimation technique was tested on both CMP and EO gathers. It was shown that δ values estimated over EO gathers were more accurate than those estimated from CMP gathers. The error analysis performed showed the dependence of parameter estimation error on the inverted NMO velocities. The values of ε estimated on the EO gathers were found to

match the model values quite well. Due to the accuracy of velocity estimation from EO gathers, these gathers are better suited for the parameter inversion. In the next Chapter, this method will be used for parameter estimation on real dataset.

Chapter 4: Field Data

4.1 Field data

The method proposed in this paper, is will next be applied on to the seismic data collected over the Blackfoot Field near Strathmore, Alberta and is located in Township 23, Range 23, West of 4th meridian, in South Central Alberta and is operated by EnCana Energy. A 3C-3D dataset was acquired at Blackfoot by the CREWES consortium in 1997.

4.2 Geology

The geology of the Blackfoot Field has been discussed in detail by Miller *et al*. (1995). The following is a very brief review of the lithology of the formations that are of interest to this work. The reservoir rocks in this field are Glauconitic incised valleys in the Lower Manville Group of the Lower Cretaceous. Coals, Viking Formation and base of fish scales shales overlie these reservoir rocks. Figures 4.1 and 4.2 show the stratigraphy in the Blackfoot region.

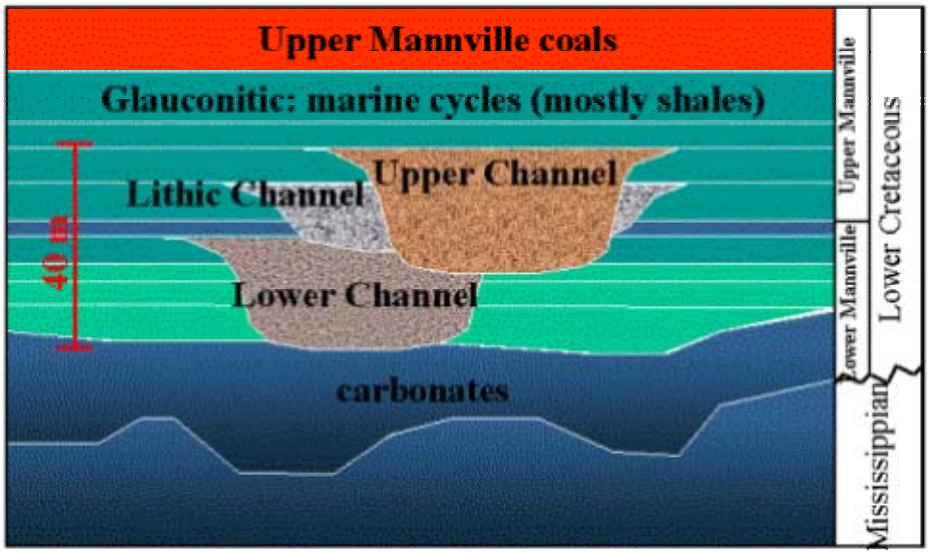

Figure. 4.1. Blackfoot Stratigraphy (Miller *et al.*, 1995).

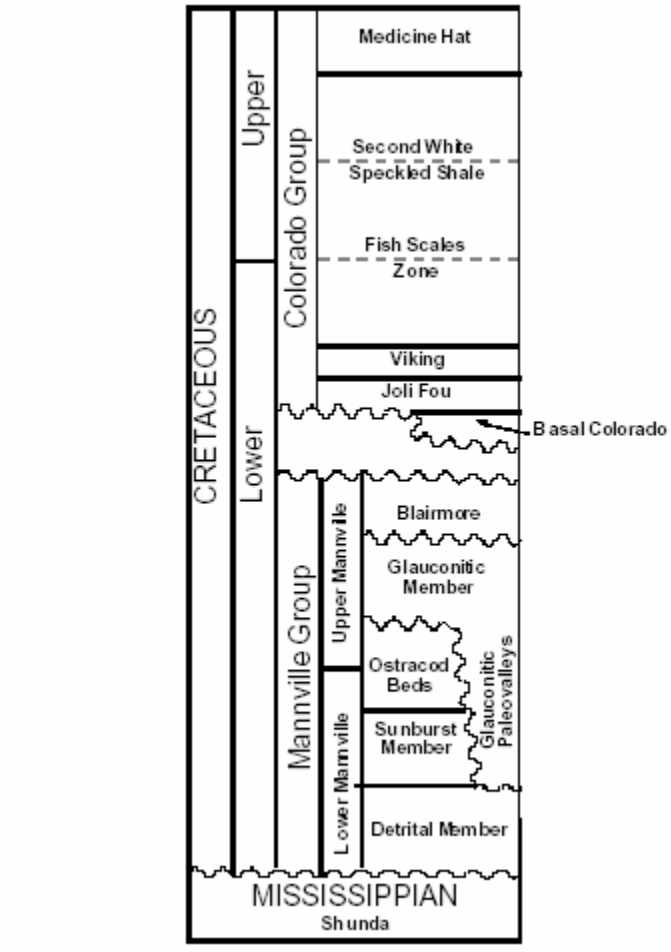

Figure 4.2. Stratigraphic sequence in the Blackfoot field (Miller *et al.*, 1995).

4.3 Seismic Survey

A line numbered '20M *vertical*' is chosen to test this method. The anisotropic analysis will be performed on both CMP and EO gathers. EO and CMP gathers are formed for this purpose at CMP 149.

The vertical velocities derived from VSP data acquired in the same area were used for the inversion for anisotropy parameters.

Monte-Carlo velocity analysis is then performed on the EO gather. The velocities estimated were used in the algorithm discussed above to estimate the values of ε and δ.

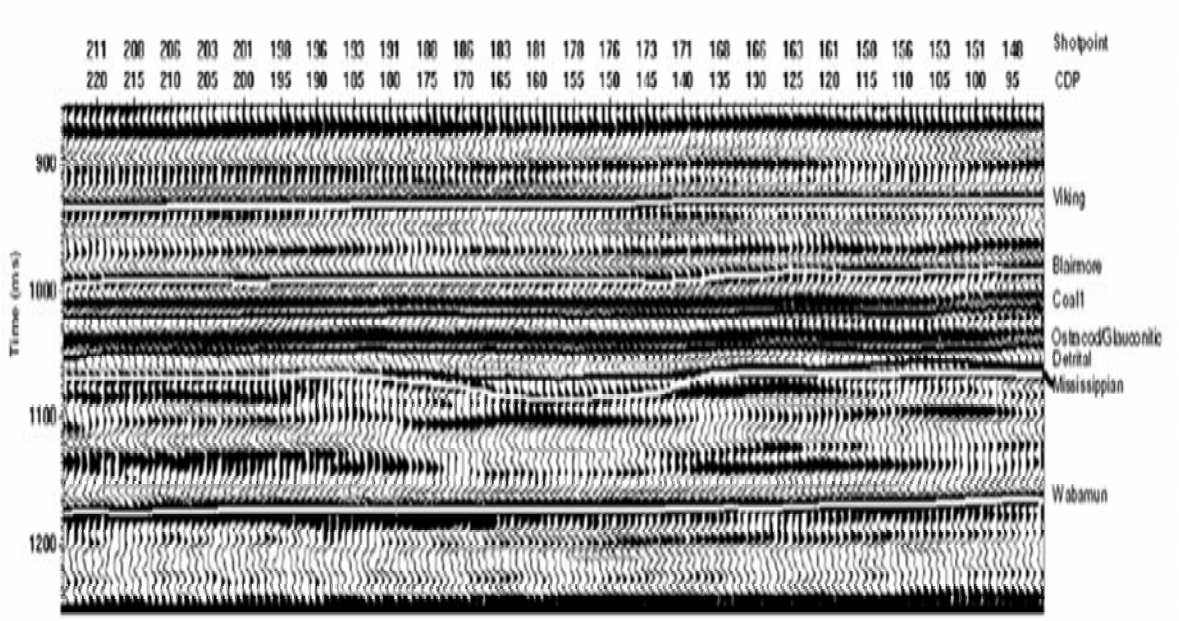

Figure 4.3. The seismic section with important horizons marked after Miller *et al.* (1995).

4.4 Anisotropy in this area

Haase (1998) studied the anisotropy in the seismic data from the western Canadian basin. He tested all the possible mechanisms and found that VTI anisotropy accounted for the observed nonhyperbolic moveout. He then carried out an anisotropic velocity analysis.

Then, using additional well log information, he computed the Thomsen anisotropy parameters by least-squares fitting with Tsvankin's (1995) anisotropic NMO equation. I made an effort to compare the values estimated by Hasse with my estimations but unfortunately in his paper he doesn't name the formations on which he estimated them on. Therefore I couldn't make an conclusive comparison.

4.5 Outline of the method

In order to apply this method to the data, basic processing flow is applied to the data which is as follows:

1. geometry allocation
2. AGC
3. band-pass filtering
4. sorting into CMP and EO gathers.

The analysis is performed on both CMP and EO gathers. The estimation can be concisely described using the following steps:

- Using the Monte Carlo inversion shifted-hyperbola is fitted to the moveout curves and V_{nmo} and S are obtained at each interval.
- Equation (4.1) is used to estimate the 'interval velocities'

$$V_{\text{int}}^2 = \frac{V_{NMO}^2(N)t_0(N) - V_{NMO}^2(N-1)t_0(N-1)}{t_0(N) - t_0(N-1)} \tag{4.1}$$

- The value of V_0, the vertical velocity is determined from the VSP data.
- Equation (4.2) is used to calculate δ_n.

$$\delta_n = \frac{1}{2}\left(\frac{V_{\text{int}}^2}{V_{0n}^2} - 1\right). \tag{4.2}$$

- Equation (4.3) is used to calculate ε_n

$$\varepsilon_n = \delta_n + \left(\frac{H_N \left(1 - k^2\right)}{8V_0^4 \left(1 - k^2 + 2\delta_n\right)} \right). \qquad (4.3)$$

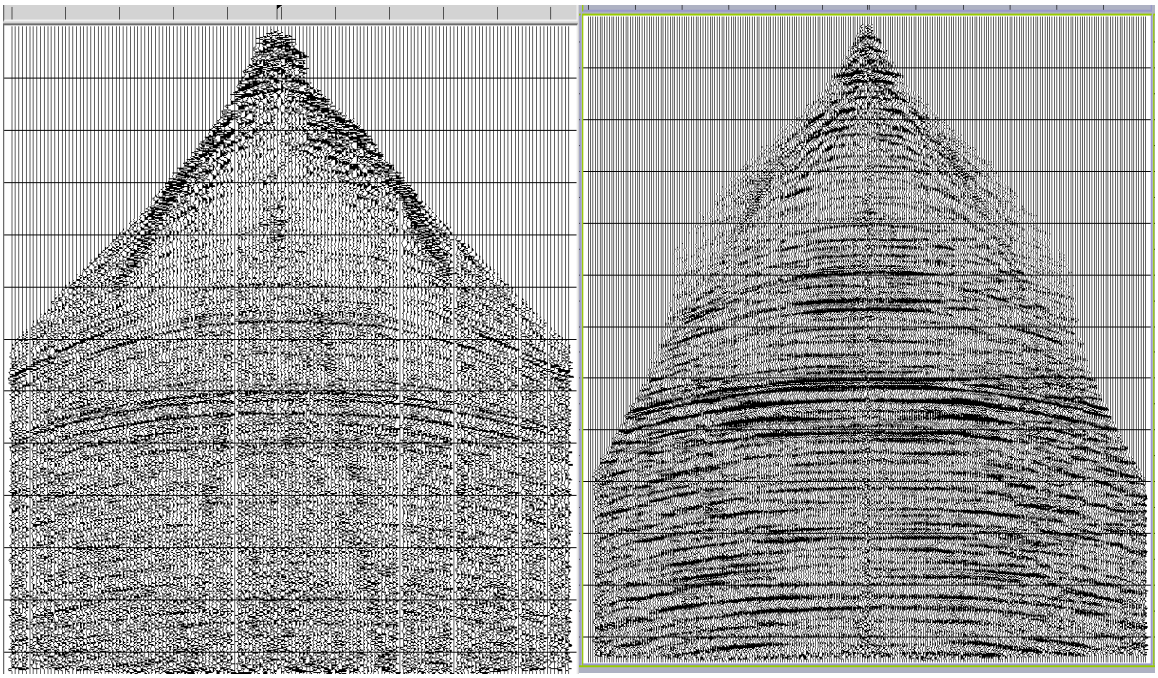

Figure 4.4. Comparison between a CMP gather and an EO gather

4.6 VSP data

A 3C-3D vertical seismic profile (VSP) is conducted in November 1995 over the Blackfoot Field. The survey is acquired in the PCP 12-16-23-23W4 well. Acquisition of the survey is performed simultaneously with the Blackfoot 3C-3D surface seismic program. A total of 431 surface shots were received by a five-level tool, set at various depths. This data is analyzed in detail by Zhang *et al.* (1996).

The interval velocities obtained from this VSP are used in the inversion. The interval velocities derived from of the VSP are of the same order as the velocities from surface seismic data as both experiments operate in the same frequency range and thus are not

dispersed. In comparison, the interval velocities estimated from well logs are slightly higher as they are measured at higher frequencies and will have more dispersion (Marion *et al*., 1994).

Dispersion can be defined as any phenomenon in which the velocity of propagation is frequency dependent. Dispersion distorts the shape of a wavetrain: peaks and troughs advance toward (or recede from) the beginning of the wave as it travels (Sheriff, 2002). In geophysical data, the well logs operate at a frequency which is an order of magnitude higher than frequencies used in surface seismic exploration. Therefore tying the velocities from the two surveys would require additional processing.

VSPs on the other hand, operate at the same frequency as that of a surface seismic survey. Using the velocities from the VSP for the estimation of anisotropy parameters will solve the problem of velocity dispersion which one encounters with the velocities from the well logs. The interval velocities derived from this VSP survey are tabulated in the Table 4.2.

In the case where VSP data is not available, the velocities from the well logs can be used after applying a sufficient dispersion correction.

The dispersion relation can be written as:

$$\kappa^2 = \kappa_x^2 + \kappa_y^2 = \omega^2 \Big/ V^2 \,, \tag{4.4}$$

where *k* is the angular wavenumber, and ω the angular frequency.

4.6 Estimation of V_{nmo} and S

The inversion technique based on the Monte-Carlo technique discussed above is applied to the moveout curves.

The important formations of interest are identified. These formations are marked on the There are tabulated in Table 4.1.

Table 4.1. Formation naming conventions

Abbreviation	Unit Name
BFS	Base of Fish Scales Zone
MANN	Blairmore-Upper Mannville
COAL	Coal Layer
GLCTOP	Glauconitic Channel porous Sandstone unit
MISS	Shunda Mississippian

The values of the shift and V_{nmo} estimated from CMP gathers and V_0 estimated from the VSP data is tabulated in Table 4.2. The same values calculated for an EO gather and VSP are tabulated in Table 4.3.

Table. 4.2. V_{NMO}, Shift, and V_0 calculated from CMP gathers

Formation	V_{NMO}	Shift (S)	$V_{0,i}$
BFS	3880	0.4687	3300
MANN	4042	0.5388	3990
COAL	4653	0.6745	3900
GLCTOP	4250	0.6764	3860
MISS	5675	0.6786	6000

Table. 4.3. V_{NMO}, Shift and V_0 calculated from EO gathers

Formation	V_{NMO}	Shift (S)	$V_{0,i}$
BFS	4002	0.6987	3300
MANN	4148	0.9388	3990
COAL	4755	0.6145	3900
GLCTOP	4460	0.8604	3860
MISS	5998	0.7256	6000

These values are the used in the parameter estimation procedure discussed in earlier chapters to estimate the anisotropy parameters. The anisotropy values calculated from the CMP gather are tabulated in Table 4.4. The values estimated from the EO gather are tabulated in Table 4.5.

Note the difference between these two tables. It is assumed from the modelling studies (Chapter 3) that estimation over EO gathers is more accurate.

Table 4.4. δ and ε values calculated using CMP gathers.

Formation	δ (estimated)	ε (estimated)
BFS	0.15	0.14
MANN	0.04	0.012
COAL	0.21	0.23
GLCTOP	0.08	0.015
MISS	0.00	0.01

Table 4.5. δ and ε values calculated using EO gathers.

Formation	δ (estimated)	ε (estimated)
BFS	0.23	0.06
MANN	0.04	0.008
COAL	0.24	0.12
GLCTOP	0.06	0.006
MISS	0.00	0.001

4.8 Conclusions and Discussions

The method for the estimation of anisotropy discussed in Chapter 2 and tested on the model data in Chapter 3 is applied to the real data acquired over Blackfoot Field in Alberta, Canada.

The data is sorted into EO gathers, as I had shown earlier that EO gathers give a better control over velocity estimation. The moveout gathers at some formations of interest were inverted using the Monte-Carlo inversion technique. This data is then used to estimate both ε and δ.

The interval velocities from VSP data were used for the inversion of anisotropy parameters. A VSP experiment is conducted in the same frequency range as that of seismic experiment and therefore these values are not affected by velocity dispersion. On the other hand, well logs which operate at a higher frequency than the surface seismic experiment are affected by this phenomenon.

After estimating the anisotropy parameters, we found that the shales and coals show significant anisotropy which is consistent with the published values (Thomsen, 1986). The sands show very little anisotropy which is also consistent with the values published in the literature (Thomsen ,1986). The values estimated here in this thesis are compared with the values estimated by Thomsen in table 4.6.

Table 4.6: Comparison between measurements presented in this thesis with those of Thomsen(1986)

Lithology	ε (estimated)	ε (Thomsen)	δ (estimated)	δ (Thomsen)
Sands	0.00	0.002-0.01	0.00	0.002-0.01
coal	0.24	0.3-0.1	0.12	0.2-0.05

Chapter 5: Conclusion and Discussion

5.1 Thesis summary

The estimation of anisotropy parameters is very important in extending the isotropic processing system and to take care of the intrinsic anisotropy of subsurface earth. There are many measures of anisotropy proposed by many authors in literature. However, the parameters ($\varepsilon, \delta, \gamma$) proposed by Thomsen in 1986, are widely used as for quantifying anisotropy. The parameters ε and δ quantify P-wave anisotropy and γ quantifies the S-wave anisotropy.

Several methods for the Thomsen anisotropy parameters' estimation have been proposed by various authors. Tsvankin, Grerchka and Alkhalifah have worked extensively in this area of anisotropic seismic processing techniques. Tsvankin in 1995, proposed a rigorous derivation for the anisotropic NMO equation, which is widely used for anisotropic NMO correction as well as for inversion for these parameters.

Tsvankin and Alkahalifah (1995) proved that the three parameters ε, δ and V_0 (the vertical velocity) cannot be estimated from the surface seismic data without any extra information. They proposed a new parameter η which is combination of ε and δ, which they proved is easily invertible along with V_0 without any extra information.

Castle (1994) proposed a shifted-hyperbola NMO (SNMO) equation, which is a better approximation to the moveout than the Dix NMO (Dix, 1955) equation. These two equations are used for the parameter estimation in this study. SNMO is exact through the

fourth order in offset while Dix's NMO equation is only a second order approximation (Castle, 1994). He also showed that the RMS velocities estimated using the SNMO, are considerably more accurate than those estimated from Dix equation. Castle's SNMO equation was used here to find a better NMO velocity and the shift parameter *S*, which was later used to find the anisotropic parameters.

The estimation procedure consists of two steps. In the first step, the parameters for normal moveout correction, V_{NMO} and the "shift parameter" are determined using Monte-Carlo inversion from both EO and CMP gathers. In the next step, the anisotropic parameters are computed from the data. A relationship that describes their dependency on the *S*, V_{NMO} and V_0 (vertical velocity) is used.

The vertical velocity is derived, in an ideal case, from VSP data as it is least affected by velocity dispersion. In the case where VSP data is not available, well log data can be used provided adequate dispersion correction is applied.

In this study, velocity analysis is performed on both the EO gathers (formally referred to as common scatter point (CSP) gathers) and CMP gather. An EO gather is a pre-stack ordering of input data that contains energy from vertical array of scatter points (Bancroft *et al*., 1998).

This method was first tested on model data generated from a model with eight flat reflectors. 'NORSAR anisotropic ray mapper' was used for the generation of

seismograms. The parameters estimated matched closely with the model parameters as shown in Figures 3.7 and Figure 3.8. The errors in the estimation of δ varied from 5-10% while the error in estimation of ε varied from 20-30%.

The δ estimation is highly dependent on the estimation of NMO velocity as shown in Figure 3.9. The error analysis of δ estimates proves how important the estimation of accurate NMO velocities is. It was shown that δ estimated using EO gathers was more accurate than when estimated using CMP gathers as illustrated in Figure 3.7.

When extending this analysis to real field data, we found that the shales and coals show significant anisotropy while the sands show very little or negligible anisotropy. Both results are consistent with the laboratory observations tabulated in Thomsen (1986).

In conclusion, a simple and robust method for the estimation of anisotropy parameters is proposed in this thesis. This method was tested and evaluated on a numerical anisotropic model. This scheme was then used over field data for the estimation of anisotropy parameters.

References

Alkhalifah, T. and Tsvankin, I., 1995, Velocity analysis for transversely isotropic media: Geophysics, **60,** 1550-1566.

Armstrong, P. N., Chmela, W. and Leaney, W. S., 1995, AVO calibration using borehole data: First Break, **13,** no. 08, 319-328.

Backus, G. E., 1962, Long-wave elastic anisotropy produced by horizontal layering: J.Geophys Res., **70**, 3429.

Bancroft, J.C., 1996, Velocity sensitivity for equivalent offset prestack migration , Ann. Mtg: Can. Soc. Expl. Geophys.

Bancroft, J.C., 2002, Practical understanding of pre and poststack migrations: Course notes.

Bancroft, J.C., Geiger, H.D. and Margrave, G.F., 1998, The equivalent offset method of prestack time migration: Geophysics, **63,** 2041-2053.

Berryman, J. G., 1979, Long-wave elastic anisotropy in transversely isotropic media : Geophysics, **44,** 896-917.

Bolshix, C. F.,1956, Approximate model for reflected wave traveltime curve in multilayered media: Applied Geophysics, **15,** 3-14, (in Russian)

Bozkurt, G., Epili, D. and Liner, C., 1999, Anisotropic tomography of the Glenn Pool crosswell data, 69th Ann. Internat. Mtg:, 239-242.

Byun, B. S. and Corrigan, D., 1990, Seismic traveltime inversion for transverse isotropy: Geophysics, **55,** 192-200.

Castle, R.J., 1994, Theory of normal moveout: Geophysics, **59,** 983-999.

Cerveny, V., 1985. The application of numerical modelling of seismic wavefields in complex structure. *Seismic shear waves,* Part A: Theory (ed. G Dhor). -124. Geophysical Press, London.

Daley, P. F. and Hron, F., 1979, Reflection and transmission coefficients for seismic waves in ellipsoidally anisotropic media: Geophysics, **44,** 27-38.

de Bazelaire, E., 1988, Normal moveout revisted –Inhomogenous media and curved interfaces: Geophysics, **53,** 142-158.

Dix, C.H., 1955, Seismic velocities from surface measurements: Geophysics, **20,** 68-86.

Grechka, V., Pech, A., Tsvankin, I. and Han, B., 2001, Velocity analysis for tilted transversely isotropic media: A physical modeling example: Geophysics, **66,** 904-910.

Grechka, V. and Tsvankin, I., 1999, NMO surfaces and Dix-type formulae in heterogeneous anisotropic media, 69th Ann. Internat. Mtg: Soc. of Expl. Geophys., 1612-1615.

Haase ,B., 1998, Non hyperbolic moveout in plains data and the anisotropy question: Recorder, Can. Soc. Expl. Geophys. Nov, 1998, 21-33.

Helbig, K., 1964, Refraction seismics with an anisotropic overburden a graphical method of interpretation: Geophys. Prosp., Eur. Assn. Geosci. Eng., **12,** 383-396.

Helbig, K., 1984, Anisotropy and dispersion in periodically layered media:Geophysics, **49,** 364-373.

Isaac, J. H. and Lawton, L. C., 1999, Image mispositioning due to dipping TI media: A physical seismic modeling study: Geophysics, **64,** 1230-1238

Le Stunff, Y., Grechka, V. and Tsvankin, I., 1999, Depth-domain velocity analysis in VTI media using surface P-wave data: Is it feasible?, 69th Ann. Internat. Mtg: Soc. of Expl. Geophys., 1604-1607.

Malovichko, A. A., 1956, A new representative of traveltime curve of reflected waves in horizontally layered media: Applied Geophysics, **91,** 47-53, (in-Russian)

Marion, D., Mukerji, T. and Mavko, G., 1994, Scale effects on velocity dispersion: From ray to effective-medium theories in stratified media:Geophysics, , **59,** 1613-1619.

Mayne, W. H., 1962, Common reflection point horizontal data stacking techniques: Geophysics, **27,** 927-938.

McCollum, B. and Snell, F. A., 1947, Asymmetry of sound velocity in stratified formations, *in* SEG Staff, Ed., Early geophysical papers, **01:** Soc. of Expl. Geophys., 216-227.

Miller, S.L.M., Aydemir, E.O. and Margrave, G.F., 1995, Preliminary interpretation of P-P and P-S seismic data from Blackfoot broad-band survey: CREWES Research Report 1995, Ch 42.

Nye, J. F.,1957, Physical properties of crystals: Oxford Press.

Ottolini, R. and Claerbout, J. F., 1984, The migration of common-midpoint slant stacks: Geophysics, **49,** 237-249.

Postma, G. W., 1955, Wave propagation in a stratified medium: Geophysics, **20,** 780-806.

Sheriff, R. E., 2002, Encyclopedic Dictionary of Exploration Geophysics, Encyclopedic dictionary of exploration geophysics: Soc. of Expl. Geophys., 384.

Siliqi, R. and Bousquié, N., 2000, Anelliptic time processing based on a shifted hyperbola approach, 70th Ann. Internat. Mtg: Soc. of Expl. Geophys., 2245-2248.

Taner, M.T. and Koehler, F., 1969, Velocity spectra - Digital computer derivation and applications of velocity functions : Geophysics, **34,** 859-881.

Thomsen, L., 1986, Weak elastic anisotropy : Geophysics, **51,** 1954-1966.

Toldi, J., Alkhalifah, T., Berthet, P., Arnaud, J., Williamson, P. and Conche, B., 1999, Case study of estimation of anisotropy: THE LEADING EDGE, **18,** no. 5, 588-593.

Tsvankin, I., 1995, Normal moveout from dipping reflectors in anisotropic media: Geophysics, **60,** 268-284.

Tsvankin, I., 1996, P-wave signatures and notation for transversely isotropic media: An overview: Geophysics, **61,** 467-483.

Tsvankin, I. and Grechka, V., 2001, Parameter estimation for VTI media using PP and PS reflection data, 71st Ann. Internat. Mtg: Soc. of Expl. Geophys., 857-860.

Tsvankin, I. and Thomsen, L., 1994, Nonhyperbolic reflection moveout in anisotropic media: Geophysics, **59,** 1290-1304

Zhang, Q., Stewart, R. R., Parkin, J. M., and Sun, Z., 1995, 3-D VSP: Analysis of the Blackfoot 3C-3D VSP survey: CREWES Project Research Report, V.8, Chpt. 40.

Appendix 1: Derivation of the equations to determine anisotropy parameters

Methodology used in the current study

Taner and Koehler (1969) gave the following generalized equation for NMO:

$$t^2 = c_0 + c_2 x^2 + c_4 x^4 + \ldots \tag{A1.1}$$

Conventional NMO of Dix truncates the above series to the second power of x (source-receiver offset) whereas Castle's algorithm extends to the fourth power in x. Castles's NMO equation, i.e. equation (2.33), can be re-written in the form of Taner and Koehler's. Coefficients in the Taylor's series are given as (denoted with superscript S):

$$c_0^{\mathrm{S}} = t_0^2, \tag{A1.2}$$

$$c_2^{\mathrm{S}} = \frac{1}{V_{\mathrm{NMO}}^2}, \tag{A1.3}$$

and

$$c_4^{\mathrm{S}} = \frac{1}{4}\frac{(1-S)}{t_0^2 V_{\mathrm{NMO}}^2} \tag{A1.4}$$

Tsvankin and Thomsen (1994) described a NMO equation for TI media in terms of the Thomsen's parameters. Their equation can be re-written in the form of Taner and Koehler's Taylor series of equation(A1.1), to yield the following Taylor series coefficients (denoted with a superscript T):

$$c_0^{\mathrm{T}} = t_0^2, \tag{A1.5}$$

$$c_2^{\mathrm{T}} = \frac{1}{V_0^2(1+2\delta)}, \tag{A1.6}$$

and
$$c_4^{\mathrm{T}} = \frac{\left(\sum_i V_{2i}^2 \Delta t_i\right)^2 - t_0 \sum_i \left(H_i + V_{2i}^4\right)\Delta t_i}{4\left(\sum_i V_{2i}^2 \Delta t_i\right)}, \tag{A1.7}$$

where H is given by

$$H = 8V_0^4(\varepsilon - \delta)\left[1 + \frac{2\delta}{(1-k^2)}\right] \quad , \tag{A1.8}$$

V_0 is the vertical velocity and k is ratio $\frac{V_p}{V_s}$.

Equating the co-efficient c_2^{S} (A1.3) with c_2^{T} (A1.6), we get the following relationship for δ:

$$\delta_n = \frac{1}{2}\left(\frac{V_{\mathrm{int}\,n}^2}{V_{0n}^2} - 1\right). \tag{A1.9}$$

Where $V_{\mathrm{int}\,n}$ is the interval NMO velocity for a particular layer and V_{0n}^2 is the vertical velocity obtained from the check shots.

Using Dix-type differentiation interval properties can be determined. According to Alkhalifah and Tsvankin, (1995), "Dix's (1955) formula makes it possible to recover the interval velocity for any particular layer from short spread moveout velocity, in flat layered isotropic media"

The interval NMO velocity $V_{\mathrm{int}\,n}$ for the N^{th} layer may be recovered using the following equation:

$$V_{\mathrm{int}\,n}^2 = \frac{V_{NMO}^2(N)t_0(N) - V_{NMO}^2(N-1)t_0(N-1)}{t_0(N) - t_0(N-1)}. \tag{A1.10}$$

Equation (A1.7) can be written in the layer stripping form as

$$\frac{1}{t_0(N)}\sum_{i-1}^{N}\left(V_{2i}^4+H_i\right)\Delta t_i = V_2^4(N)\left[1-4C_4^t(N)t_0^2(N)V_2^4(N)\right] \qquad \text{(A1.11)}$$

(Alkhalifah and Tsvankin, 1995).

The equation (A1.11) can be written as

$$F(N) = V_2^4(N)\left[1-4C_4^s(N)t_0^2(N)V_2^4(N)\right] \qquad \text{(A1.12)}$$

(Alkhalifah and Tsvankin, 1995).

Note that $C_4^t(N)$ has been replaced by $C_4^s(N)$.

Where $F(N)$ is thus a known function of the Taylor series coefficients for the reflection from the *N*th boundary. $C_3^s(N)$ can be calculated using the following equation:

$$C_4^s(N) = \frac{1}{4}\frac{(1-S)}{t_0^2 V_{NMO}^2}. \qquad \text{(A1.13)}$$

Now, using the values of $F(N)$ and $F(N-1)$, $H(N)$ can be calculated as follows

$$H_N = \frac{F(N)t_0(N)-F(N-1)t_0(N-1)}{t_0(N)-t_0(N-1)} \qquad \text{(A1.14)}$$

(Alkhalifah and Tsvankin, 1995).

But we know that H_N is given by the equation (A1.8)

The equation (A1.8) can be rewritten as the equation

$$\varepsilon_n = \delta_n + \left(\frac{H_N\left(1-k^2\right)}{8V_0^4\left(1-k^2+2\delta_n\right)}\right). \qquad \text{(A1.15)}$$

Using equations (A1.9) and (A1.15) ε and δ can be estimated at each of the layers.

Appendix 2: Monte-Carlo inversion

The shifted hyperbola equation is a non-linear problem so linear inversion techniques (e.g. least-squares inversion) usually fail. A random walk technique like Monte-Carlo inversion would serve the purpose of inverting the moveout equation (2.37) for both S and V_{nmo}.

Monte-Carlo Inversion

Monte-Carlo methods are random search methods in which the models are drawn randomly from the whole model space and tested against the data. The best model depending on the acceptance criteria is then considered as the solution to the inversion problem.

In this inversion procedure each model parameter in the model-parameter set **m** is allowed to vary within a predefined search interval (determined a priori or by trial and error). Therefore for each model parameter m_i, we define

$$m_{\mathrm{i}}^{\min} \leq m_i \geq m_{\mathrm{i}}^{\max} \qquad \text{(A2.1)}$$

The method can be described by equation (A2.2) for a model parameter set

m (S, V_{NMO}),

$$m_{\mathrm{i}}^{\mathrm{new}} = m_{\mathrm{i}}^{\min} + (r_{\mathrm{n}})\left[m_{\mathrm{i}}^{\max} - m_{\mathrm{i}}^{\min} \right]. \qquad \text{(A2.2)}$$

Where m_i^{new} is the new model parameter m_i^{min} , m_i^{max} are the minimum and maximum values of the model parameter specified and 'r_n' is a random number drawn from a uniform distribution [0,1].

The generated models m_i^{new} are tested iteratively. The generated model that best fits the data with a minimum misfit is accepted. The algorithm may be represented as the following series of operations.

1. Generate a new model set **m** using equation (A2.2).

2. Calculate $t(x_m)$ (the model traveltime) at every offset using equation (2.33)

3. Calculate the difference 'ξ' between the model travel time $t(x_m)$ and data travel time $t(x_d)$ at each offset.

4. Count the number of offsets N whose ξ values fall under acceptable limits.

5. If N is acceptable the model set **m** is accepted; if not steps 1-4 are repeated.